Neurobiology of Disease 73 (2015) 254–268

Contents lists available at ScienceDirect

Neurobiology of Disease

journal homepage: www.elsevier.com/locate/ynbdi

SEMA4D compromises blood–brain barrier, activates microglia, and inhibits remyelination in neurodegenerative disease

Ernest S. Smith [a], Alan Jonason [a], Christine Reilly [a], Janaki Veeraraghavan [a], Terrence Fisher [a], Michael Doherty [a], Ekaterina Klimatcheva [a], Crystal Mallow [a], Chad Cornelius [a], John E. Leonard [a], Nicola Marchi [b], Damir Janigro [b], Azeb Tadesse Argaw [c], Trinh Pham [c], Jennifer Seils [a], Holm Bussler [a], Sebold Torno [a], Renee Kirk [a], Alan Howell [a], Elizabeth E. Evans [a], Mark Paris [a], William J. Bowers [a], Gareth John [c], Maurice Zauderer [a,*]

[a] Vaccinex, Inc., Rochester, NY 14620, USA
[b] Cerebrovascular Research Center, Department of Molecular and Cellular Biology, Cleveland Clinic Lerner College of Medicine, Cleveland, OH 44195, USA
[c] Corinne Goldsmith Dickinson Center for Multiple Sclerosis, Department of Neurology, Mount Sinai School of Medicine, New York, NY 10029, USA

ARTICLE INFO

Article history:
Received 8 July 2014
Revised 2 October 2014
Accepted 12 October 2014
Available online 18 October 2014

Keywords:
Remyelination
Neuroinflammation
Monoclonal antibody
Semaphorin-4D
Oligodendrocytes
Multiple sclerosis
Blood–brain barrier

ABSTRACT

Multiple sclerosis (MS) is a chronic neuroinflammatory disease characterized by immune cell infiltration of CNS, blood–brain barrier (BBB) breakdown, localized myelin destruction, and progressive neuronal degeneration. There exists a significant need to identify novel therapeutic targets and strategies that effectively and safely disrupt and even reverse disease pathophysiology. Signaling cascades initiated by semaphorin 4D (SEMA4D) induce glial activation, neuronal process collapse, inhibit migration and differentiation of oligodendrocyte precursor cells (OPCs), and disrupt endothelial tight junctions forming the BBB. To target SEMA4D, we generated a monoclonal antibody that recognizes mouse, rat, monkey and human SEMA4D with high affinity and blocks interaction between SEMA4D and its cognate receptors. In vitro, anti-SEMA4D reverses the inhibitory effects of recombinant SEMA4D on OPC survival and differentiation. In vivo, anti-SEMA4D significantly attenuates experimental autoimmune encephalomyelitis in multiple rodent models by preserving BBB integrity and axonal myelination and can be shown to promote migration of OPC to the site of lesions and improve myelin status following chemically-induced demyelination. Our study underscores SEMA4D as a key factor in CNS disease and supports the further development of antibody-based inhibition of SEMA4D as a novel therapeutic strategy for MS and other neurologic diseases with evidence of demyelination and/or compromise to the neurovascular unit.

Introduction

Multiple sclerosis (MS) is a neuroinflammatory disease triggered by immune-mediated damage to neuronal myelin sheaths in the brain, spinal cord, and optic nerve. Demyelination resulting from periodic disease relapses eventually leads to disrupted axonal signal transduction and debilitating loss of motor function. Disease progression is difficult to predict, as it depends on the subtype of the disease (relapsing–remitting, secondary progressive, primary progressive, and progressive relapsing), and is subject to individual variation in the severity of initial symptoms and disease progression.

Although the agents and stimuli that initiate disease are presently unknown, certain cellular and molecular processes relating to immune system dysfunction, neuroinflammation, myelin damage and repair, and blood–brain barrier (BBB) compromise have been shown to significantly contribute to the pathophysiology of MS. Disease-related lesions, which are characterized by focal loss of myelin (Prineas, 1975), lymphocytic and macrophage infiltrates, and activated microglia and astrocytes, are scattered throughout the CNS, but are found at highest frequencies in the brainstem, optic nerve, spinal cord, and periventricular white matter (Adams, 1977). Autoreactive T cells, especially those with Th1 and Th17 signatures, are believed to be primary drivers of monocyte recruitment, oligodendrocyte toxicity, and myelin destruction (Pierson et al., 2012). BBB compromise in MS patients is detectable not only in focal lesions, but also in diffuse white matter abnormalities identified by postmortem MRI, suggesting that dysfunction in BBB may be a significant contributor to disease pathology (Vos et al., 2005).

While no cure for MS currently exists, therapeutics developed to specifically target one or more of these mechanisms have shown promise in reducing symptom severity and relapse frequencies. Many of the currently FDA-approved medications are directed against the immune component of MS via targeted immunosuppression to prevent autoreactive T cells from entering the CNS and degrading myelin integrity. Such strategies, while moderately effective, can have significant

* Corresponding author at: Vaccinex, Inc., 1895 Mt. Hope Avenue, Rochester, NY 14620, USA. Fax: +1 585 271 2765.
E-mail address: mzauderer@vaccinex.com (M. Zauderer).
Available online on ScienceDirect (www.sciencedirect.com).

http://dx.doi.org/10.1016/j.nbd.2014.10.008

side-effects (Brinkmann et al., 2010; Kappos et al., 2010; Hohlfeld et al., 2011; Miller et al., 2003; Berger, 2010).

There is a need to identify and rigorously test new strategies that may intercede at multiple other points in MS pathogenesis and that may effectively slow or even reverse progression of this debilitating disease. One such novel molecular target known to participate in several processes affecting MS pathology, including inflammation, cellular migration, oligodendrocyte viability, and endothelial cell cytoarchitecture, is semaphorin 4D (SEMA4D). Semaphorins comprise a family of soluble and membrane-bound proteins that were originally defined as axon-guidance factors (reviewed by Giger et al., 2010). These proteins play important roles in establishing precise connections between neurons and their appropriate targets. Semaphorins and their receptors have also been shown to have important functions in other physiological processes in the adult organism, including tissue repair, activation and migration of endothelial cells, survival and differentiation of neuronal and oligodendrocyte precursor cells, tumor progression, and immune cell regulation (Basile et al., 2007; Ch'ng and Kumanogoh, 2010; Giordano et al., 2002; Giraudon et al., 2004; Suzuki et al., 2008). SEMA4D is a 150-kDa transmembrane protein expressed on the surface of T and B cells, monocytes, platelets, and professional antigen-presenting cells, such as dendritic cells (Kikutani and Kumanogoh, 2003; Suzuki et al., 2008). Cellular activation can result in the generation of soluble SEMA4D (sSEMA4D) by proteolytic cleavage of the extracellular portion of transmembrane SEMA4D (Hall et al., 1996; Zhu et al., 2007). Levels of sSEMA4D in normal mouse, rat, and human sera are similar, typically ranging from 10 to 20 ng/mL (manuscript in preparation). Both membrane-associated and soluble forms of SEMA4D are biologically active.

Three cellular receptors have been identified for SEMA4D: Plexin-B1 (PLXNB1), Plexin-B2 (PLXNB2), and CD72. PLXNB1, the highest-affinity SEMA4D receptor ($K_D = 1$ nM), is expressed in multiple tissues, including dendritic cells, endothelial cells, and neural cells (Tamagnone et al., 1999). SEMA4D engagement with PLXNB1 has been shown to induce activation and migration of endothelial cells, and to promote migration of tumor cells (Conrotto et al., 2005; Giordano et al., 2002). SEMA4D/PLXNB1 signaling has also been reported to induce growth cone collapse in neurons, apoptosis of neural precursor cells, and process extension collapse and apoptosis of oligodendrocytes (Giraudon et al., 2004; Giraudon et al., 2005; Basile et al., 2007; Liang et al., 2004; Niederost et al., 2002). PLXNB2 has an intermediate affinity for SEMA4D and a recent report indicates that PLXNB2 regulates migration of cortical neurons independently of PLXNB1 (Azzarelli et al., 2014). CD72 is a relatively low-affinity ($K_D = 300$ nM) SEMA4D receptor (Kumanogoh et al., 2000) expressed on B cells, APCs and platelets. Agonistic anti-CD72 antibodies exhibit many of the same effects as sSEMA4D, such as enhancement of CD40-induced B cell responses and B cell shedding of CD23. In addition, CD72 is thought to act as a negative regulator of B cell responses by binding the tyrosine phosphatase SHP-1, which can recruit many inhibitory receptors. An interaction between SEMA4D and CD72 leads to the dissociation of SHP-1, and loss of this negative activation signal (Kumanogoh and Kikutani, 2001).

Inhibition of SEMA4D could have a profound impact on the course of MS due to its multiple functions in health and disease. First, given the role of SEMA4D in inflammatory processes, inhibition of this semaphorin could quell inflammation and secondary immune responses to CNS-derived antigens (Okuno et al., 2010). Second, because SEMA4D has been shown to be toxic to the oligodendrocyte lineage as well as inhibiting migration and differentiation (Giraudon et al., 2004), blocking its activity could reduce the loss of oligodendrocyte precursor cells (OPC) and promote remyelination and repair in the setting of MS. Finally, SEMA4D inhibition may preserve the integrity of the neurovascular unit comprised of endothelial cells, pericytes and astrocytes by protecting endothelial tight junctions (Basile et al., 2005; Yang et al., 2011), this could serve to not only reduce immune and inflammatory cell infiltration into the CNS but also to prevent activation of astrocytes and microglia. To efficiently target SEMA4D, we generated a monoclonal antibody that recognizes SEMA4D from several species with high affinity and blocks interaction between SEMA4D and all of its known receptors, PLXNB1, PLXNB2, and CD72. We employed a series of in vitro analyses and in vivo models to show that antibody-based inhibition of SEMA4D is effective in blocking the deleterious effects of this semaphorin on the oligodendrocyte lineage and on BBB integrity. We demonstrate in vivo that antibody to SEMA4D significantly attenuates the severity of experimental autoimmune encephalomyelitis (EAE) in multiple rodent models, and promotes OPC migration to the site of lesions and repair following chemically induced demyelination.

Materials and methods

Animals

Mice

All mouse EAE experiments were carried out according to the guidelines of the National Institute of Health (NIH) and the University Committee on Animal Resources (UCAR) at the University of Rochester (Rochester, NY) for the care and use of laboratory animals. Female mice (C57BL/6 and SJL) weighing 25–35 g were purchased from Taconic and Charles River. All mice were housed at a standard temperature (22 ± 1 °C) on a 12-h light/dark cycle and were allowed food and water ad libitum. *Rats*: All rat EAE and lysolecithin-induced spinal cord lesion experiments were carried out at Charles River-Discovery Research Services (Kuopio, Finland) according to the National Institute of Health (NIH) guidelines for the care and use of laboratory animals, and approved by the National Animal Experiment Board, Finland. Eight week-old female Dark Agouti (DA) rats weighing 120–170 g and purchased from Charles River Laboratories, Germany, were used in a subset of EAE experiments. Male Sprague–Dawley rats at the age of 8 weeks purchased from Charles River Laboratories, Germany, were used for the lysolecithin lesion experiment. Animals were housed at a standard temperature (22 ± 1 °C) on an 11/13-h light/dark cycle with ad libitum access to food and water.

EAE models

Induction of active EAE in SJL mice

EAE was induced in 8 week-old female SJL/J mice (Charles River, Wilmington, MA) by immunizing with 0.1 mg $PLP_{139–151}$ (Anaspec, Fremont, CA) in 0.1 ml complete Freund's adjuvant (CFA; Hooke Laboratories, Lawrence, MA), subcutaneously and divided between four sites on the back of each mouse. Anti-SEMA4D antibody (MAb 67-2) or control IgG antibody (MAb 2B8) was administered intraperitoneally (i.p.) on day 7 and weekly thereafter (0.6 mg/injection; 18 mice/group). Disease progression was monitored by body mass and clinical assessment using a 6-point scoring system: (1) limp tail, (2) righting reflex is impaired, (3) ataxia, (4) early paraparesis, (5) full paralysis, and (6) moribund/death. Animals were euthanized when observed to attain score = 5. Group mean was calculated at each time point; a score of 5 was carried over into later time points following death. Two-way ANOVA was employed to analyze statistical significance of treatment.

Adoptive transfer EAE in SJL mice

EAE was induced as described above in donor mice and, 10 days later, $CD4^+$ T cells were isolated from spleens and lymph nodes of the donor EAE mice (negative selection, Miltenyi Biotec, Cambridge, MA) and cultured at a concentration of 2×10^6 cells/ml in RPMI 1640 medium supplemented with 10% FBS, 4 mM L-glutamine, 10 mM non-essential amino acids, 1 mM sodium pyruvate, 100 U/ml penicillin/streptomycin and 50 μM 2-mercaptoethanol in the presence of irradiated (3400 rad) antigen presenting cells (APC) (APC:T cell ratio = 3:1). To enrich for Th1 cell differentiation (Axtell et al., 2010; Jager et al., 2009), cells were stimulated with 20 μg/ml $PLP_{139–151}$, 20 μg/ml anti-

murine IL-4 (Clone 11B11) (BioXcell, West Lebanon, NH) and 10 ng/ml murine IL-12 (R&D systems, Minneapolis, MN). After 72 h, cells were collected, resuspended in media containing 20 μg/ml $PLP_{139–151}$ and 20 U/ml (1.82 ng/ml) murine IL-2 (R&D systems, Minneapolis, MN) and cultured on freshly irradiated splenocytes from naïve SJL/J mice for an additional 5 d, followed by re-stimulation in the presence of 1 μg/ml anti-CD3 (Clone 145-2C11) and 0.5 μg/ml anti-CD28 (Clone PV-1) for 48 h. Th1 cells were collected and 2×10^6 cells were injected i.p. into naïve SJL/J donors. To assess population purity, the remaining Th1 cells were stimulated with 50 ng/ml PMA (Sigma, St Louis, MO) and 1 μM ionomycin (Sigma, St Louis, MO) for 4.5 h and supernatants were analyzed by ELISA for the presence of Th1-specific cytokine, IFNγ (data not shown). Anti-SEMA4D antibody (MAb 67-2) or control IgG antibody (MAb 2B8) was administered i.p. on the same day as adoptive transfer and twice weekly thereafter (0.6 mg/injection; 12 mice/group). The treatment with recombinant murine IFN-β (PBL Interferon Source, Piscataway, NJ) consisted of i.p. injections of 1000 U three times a week starting on the day of the adoptive transfer. Disease progression was monitored as described above.

Induction of EAE in C57BL/6 mice

EAE was induced in naïve ~8 week-old (18–22 g) male C57BL/6 mice by immunization with emulsion containing 0.15 mg $MOG_{35–55}$ in CFA enriched with *Mycobacterium tuberculosis* (4 + 1 = 5 mg/mL CFA) in a volume of 0.2 ml/mouse, injected subcutaneously into the flank. Anti-SEMA4D antibody (MAb 67-2) or control IgG antibody (MAb 2B8) was administered i.p. on day 7 and twice weekly thereafter (0.6 mg/injection; 14 mice/group). Disease progression was monitored by body mass and clinical assessment using a 6-point scoring system: (1) limp tail, (2) righting reflex is impaired, (3) ataxia, (4) early paraparesis, (5) full paralysis, and (6) moribund/death. Group mean was calculated at each time point; a score of 6 was carried over into later time points following death. Two-way ANOVA was employed to analyze statistical significance of treatment.

Induction of EAE in DA rats

EAE was induced in female Dark Agouti (DA) rats (Charles River, Germany) by administration of 100 μL inoculum intradermally at the base of the tail. The inoculum consisted of 20 μg of recombinant $MOG_{1–125}$ (Anaspec, Australia) in PBS emulsified with incomplete Freund's adjuvant (IFA) (1:1) containing 200 μg of heat-inactivated *M. tuberculosis* (strain H 37 RA; Difco, Detroit, MI). Anti-SEMA4D antibody (MAb 67-2) or control IgG antibody (MAb 2B8) was intravenously administered at 15 mg/kg on days 3, 7, 10, 14, 21 and 28 (30 rats/group). Disease progression was monitored by body mass and clinical assessment using a 5-point scoring system: (1) tail paralysis; (2) partial weakness in one limb (usually hind limb); (2.5) complete paralysis in one limb − (no movement preserved in affected limb); (3) partial weakness in both hind limbs; (3.5) complete paralysis in both hind-limbs (hind-limbs dragged along), or partial weakness in limbs on one side of the body (hemiparesis); (4) partial weakness in all four limbs or complete paralysis on one side of the body (hemiplegia); and (5) complete paralysis of all four limbs (tetraplegia), moribund. Animals were euthanized when observed to attain score = 5. Group mean was calculated at each time point; a score of 5 was carried over into later time points following death. Two-way ANOVA was employed to analyze statistical significance of treatment.

High-resolution frequency analysis of cytokine-secreting mouse splenocytes by enzyme-linked immunosorbent spot (ELISPOT) assay

Mouse IFNγ and interleukin-17a ELISPOT "READY-SET-GO!" Kits from eBioscience (San Diego, CA) were used according to the manufacturer's protocol. Mononuclear cells from spleens of mice immunized with $PLP_{139–151}$ peptide were recall-activated in triplicate 96-well U-bottom Multi-screen filter plates with Immobilon-P membranes (Millipore, Billerica, MA). 96-Well polyvinylidene difluoride (PVDF) membrane ELISPOT plates were pre-coated with the respective anti-cytokine capture antibodies and mouse splenocytes were incubated at a cell density of 2.5×10^6 cells/ml with $PLP_{139–151}$ peptide at 25 μg/ml for 20 h at 37 °C. Cells in control wells were incubated with medium alone (RPMI, 10% FBS, non-essential amino acids, 15 mM HEPES and 15 μg/ml gentamicin) in the absence of recall peptide. Cells were washed off and the ELISPOT SET protocol followed to perform the assay. Spots were developed to the optimal intensity, and air-dried plates were scanned and analyzed by Cellular Technology Ltd. (Shaker Heights, OH).

CFSE splenocyte proliferation assay

CellTrace CFSE Cell Proliferation Kit (Invitrogen, Grand Island, NY) was used according to the manufacturer's instructions. Briefly, mononuclear cells (MNCs) isolated from spleens of treated mice were resuspended to a final concentration of 2×0^6 cells/ml in PBS, 1% BSA. Cells were stained with 10 μM CFSE dye for 15 min at 37 °C with occasional mixing. Staining was then quenched by the addition of 5 volumes of ice cold PBS/BSA and subsequent washing of the cells. Cells were resuspended to a final concentration of 2×0^6 cells/ml in complete DMEM (DMEM, 10%FBS, pen-strep, L-Glutamine, nonessential amino acids, HEPES, 50 μM 2-ME). Cells were restimulated in culture with $PLP_{139–151}$ (50, 500, or 5000 ng/ml), PMA/ionomycin cell stimulation cocktail (eBioscience, San Diego, CA), or media alone. All culture conditions were set up in triplicate in 96-well U bottom plates. On day 4, triplicate wells were pooled and cells were harvested, washed with PBS, 1% BSA and then stained with mouse anti-CD3-APC clone 145-2C11 (eBioscience, San Diego, CA). Samples were gated on $CD3^+$ cell population and 20,000 events acquired using FACSCanto™II flow cytometer. FlowJo version 7.6 was used for data analysis of CFSE fluorescence.

Cytometric bead array (CBA) cytokine analysis

MNCs were isolated from brains and spinal cords of treated animals following perfusion with PBS/heparin. Tissues were separated into small pieces using a scalpel and syringe plunger and the tissue homogenate was pressed through a 70-μm cell strainer and washed with ice-cold PBS. Samples were pooled within each treatment group and MNCs isolated by a 30%:70% Percoll (Sigma, St Louis, MO) gradient. Isolated cells were then washed and stimulated for 4 days using culture conditions for cell proliferation. On day 4, culture supernatants were collected and stored at -80 °C for subsequent analysis. Fifty microliters of each sample was analyzed for IL-2, IL-4, IL-6, IL-10, IL-17, TNFα and IFNγ using BD's mouse TH1/TH2/TH17 CBA kit and a FACSCanto™II flow cytometer. CBA sample analysis was completed following kit instructions. Statistical analysis software GraphPad Prism 5 was used for graphing of standard curves and extrapolation of data.

Immunohistochemistry for mouse B cells, T cells, and macrophage/microglia

For B cells, 5-μm PFA-fixed, paraffin-embedded sections were deparaffinized using Xylenes baths and rehydrated with graded ethanol baths. Epitope retrieval was carried out by a 20-min boil with Target Retrieval Solution (Dako, Carpinteria, CA) followed by 30-min cooling. Slides were washed twice with PBS containing 0.05% Tween-20 (TPBS), then endogenous peroxidases were inactivated with a 10-min block with Dual Enzyme Block (Dako, Carpinteria, CA). Slides were washed with TPBS twice, and nonspecific binding was blocked by a 20-min incubation with 2.5% normal goat serum in TPBS. Following a single TPBS wash, slides were incubated for 60 min with rat anti-CD45R (R&D systems, Minneapolis, MN) (clone RA3-6B2) at 0.3 μg/ml in TPBS, followed by 2 TPBS washes. Slides were then incubated for 10 min with Polink-2 rat enhancer (Golden Bridge, Mukilteo, WA) followed by 10 min with Polink-2

HRP Polymer, washing 3× with TPBS between steps. This was followed by a 5-min DAB + incubation (Dako, Carpinteria, CA). Sections were counterstained with Harris hematoxylin, destained, blued with tap water, dehydrated, and non-aqueous mounted with Permount. For detection of macrophage/microglia, staining was performed as above, using rat anti-F4/80 (Abcam, Cambridge, MA) (clone A3-1) at 0.5 μg/ml. For T cell detection, staining was performed as above, with the following changes: primary antibody was rabbit anti-CD3 (Abcam, Cambridge, MA) at 2 μg/ml. In addition, Polink enhancer and Polink HRP-Polymer incubations were replaced by one 20-min incubation with Envision + anti-rabbit HRP polymer (Dako, Carpinteria, CA). Slides were imaged at 20× magnification using a Retiga QICAM-12 bit camera coupled to an Olympus Ix50 microscope.

Evaluation of anti-SEMA4D in the rat influenza viral clearance model

Anti-SEMA4D was evaluated for immune suppression in an influenza host resistance model in Sprague Dawley, CD male and female rats by measuring viral clearance in lung homogenates. Anti-SEMA4D (VX15/MAb 2503) was delivered at 5 weekly intravenous doses of 10, 100, or 200 mg/kg prior to virus infection and 3 weekly doses subsequent to infection (25 males and 25 females per group). A vehicle control group was dosed similarly to serve as a negative control and dexamethasone was administered at 2 mg/kg/day to a separate cohort to serve as a positive control for immune suppression. After 5 doses of anti-SEMA4D rats were infected intranasally with a rat-adapted influenza virus (approximately 2×10^5 plaque forming units) to determine whether anti-SEMA4D inhibited the rat's ability to clear virus. For the infection, animals were anesthetized with isoflurane and infected intranasally with an H3N2 rat-adapted influenza virus (RAIV) as a 1:100 dilution of the stock virus (approximately 2×10^5 plaque forming units) in a volume of 200 μl. Animals that sneezed or snorted the dose immediately after the intranasal administration received a second 100 μl intranasal dose of the infection suspension as soon as possible after the first dose was attempted. On days 1, 2, 4, 8, and 21 post-infection, animals were euthanized and infectious virus titers were determined. Whole-lung homogenates were prepared at 10% w/v, split into aliquots, and stored frozen at −70 °C. Dilutions of the animals' whole lung homogenate (each performed in duplicate) were added to monolayers of Madin Darby Canine Kidney (MDCK) cells and covered with an agarose overlay. Following incubation for 36–48 h to allow plaque development, the cell monolayers were fixed with buffered formalin and stained with crystal violet. Viral plaques were counted visually to determine infectious virus titer and expressed as log plaque-forming units (PFU) per gram of lung tissue.

DIV–BBB model

A dynamic in vitro blood–brain-barrier model (DIV–BBB) was used as previously described (Cucullo et al., 2011). Briefly, a bundle of hollow fibers was suspended inside a sealed chamber and flow of cell culture medium was maintained throughout the experiment. Human cerebral endothelial cells were cultured on the luminal (vascular) side of these fibers and human astrocytes were cultured on the outer (CNS) surface. Ports positioned on both the luminal and the abluminal sides allowed access to both compartments. Once a tight barrier was established as determined by transendothelial electrical resistance (TEER), usually after 14 days, recombinant SEMA4D was added to the luminal side at various concentrations followed by either anti-SEMA4D (VX15/2503) or control IgG (MAb 2955) and the integrity of the barrier was continually monitored by measuring the transendothelial electrical resistance (TEER).

Primary mouse brain microvascular endothelial culture analyses

C57BL/6 mouse brain microvascular endothelial cells (mBMVECs; CellBiologics, Chicago, IL) were seeded onto gelatin-coated wells and grown to confluence for 5 days to allow for tight junction formation, with media changes on days 2 and 4. Cells were then treated in triplicate wells with media alone, 100 ng/ml recombinant TNFα (Millipore, Billerica, MA), or recombinant mouse SEMA4D for 6 or 12 h. For Western blotting, the wells were washed with cold PBS and scraped into 200 μl of ice-cold lysis buffer (50 mmol/L Tris pH 7.5, 4 mmol/L EDTA, 10% ethylene glycol, 250 mmol/L sucrose, 1 mmol/L dithiothreitol, 1× protease inhibitor cocktail (Roche, Indianapolis, IN), as previously described (Errede et al., 2012). Lysates were sonicated on ice for 15 s, and then frozen at −20 °C. Prior to gel loading, samples were thawed on ice and pelleted by centrifugation at 13,000 RPM for 10 min. To 65 μl lysate supernatant, 25 μl NuPAGE buffer and 10 μl reducing agent were added, then the samples were heated at 70 °C for 5 min. Each sample (15 μl) was loaded on a NuPAGE gel and run at 150 V for 1.5 h, then transferred to PVDF for 7 min using an iBlot system (Invitrogen, Grand Island, NY). Blots were blocked with 5% milk in PBS/0.05% Tween-20 overnight at 4 °C, then probed for Claudin-5 (Abcam, Cambridge, MA) or β-actin (Cell Signaling Technology, Danvers, MA) for 1 h at RT, followed by HRP-labeled goat anti-rabbit IgG H + L (Jackson ImmunoResearch, West Grove, PA) for 30 min at RT. Signal was developed using ECL Prime (GE Healthcare Life Science, Pittsburgh, PA) and imaged using a FluorChem HD2 imaging system (Alpha Innotech, Johannesburg, SA). Densitometry was calculated using NIH ImageJ. For immunofluorescence, cells were washed with PBS and fixed for 20 min with 4% paraformaldehyde in PBS with 0.05% Tween-20 (TPBS). Cells were permeabilized for 30 min with 0.05% Saponin (Sigma, St. Louis, MO) in TPBS, washed, and subsequently blocked with 2.5% normal goat serum (Jackson ImmunoResearch, West Grove, PA). Cells were incubated with 10 μg/ml mouse anti-Claudin-5 (Invitrogen, Grand Island, NY) for 60 min, washed, then incubated with a 1:500 dilution of donkey anti-mouse secondary (Invitrogen, Grand Island, NY) and washed. Slides were then labeled for 10 min with 500 ng/ml DAPI, washed, and mounted using Prolong Gold mounting medium (Invitrogen, Grand Island, NY).

Fibrinogen detection

For detection of fibrinogen, a rabbit anti-fibrinogen antibody (Dako, Carpinteria, CA) was used. Briefly, frozen sections were allowed to reach room temperature for 20 min and hydrated with PBS for 1 min. Slides were washed with PBS and blocked for 30 min with PBS containing 10% goat serum, 0.3% Triton X-100. Primary antibodies (anti-fibrinogen at 1:1000) were added and incubated overnight at 4 °C. Slides were washed rigorously with PBS containing 0.3% Triton X-100, then incubated 1 h at RT with Alexa-488 goat anti-rabbit (Invitrogen, Grand Island, NY) diluted at 1:100 in blocking buffer. Slides were washed with PBS containing 0.3% Triton X-100 and mounted with DAPI Fluoromount-G (Southern Biotech, Birmingham, AL).

Detection of therapeutic antibody in the brain via flow cytometry

SJL mice induced with $PLP_{139–151}$ peptide and CFA were injected with 600 μg of VX15/2503 or control IgG. Two days later, brains were harvested from perfused mice and processed for mononuclear cells using Percoll gradient (56). A naïve SJL mouse was included as a control. For each condition, staining was done to determine the expression (measured as percent saturation) of SEMA4D on $CD3^+$ T lymphocytes using 3 sample tubes processed in parallel. The first tube served as a negative isotype control and was incubated with mouse anti-chicken IgG-biotin (Southern Biotech, Birmingham, AL). The second tube was the experimental sample and was incubated with mouse anti-human IgG4-biotin (Southern Biotech, Birmingham, AL). This sample indicated the amount of VX15/2503 bound to surface SEMA4D on the cells. The third tube was a positive control used to measure the maximum amount of possible VX15/2503 on the surface of the cells. This tube was incubated with excess VX15/2503 followed by mouse anti-human

IgG4-biotin. All three tubes received FITC-conjugated rat anti-mouse CD3 antibody (clone 17A2) (BD, San Jose, CA) and Streptavidin-APC (Southern Biotech, Birmingham, AL), and 5000 gated $CD3^+$ events were acquired on a BD FACSCanto II™ cytometer. The geometric mean fluorescence intensity (GMFI) was determined on the T cell population. Percent saturation was calculated with the following equation: ((GMFI Tube 2 − GMFI Tube 1) / GMFI Tube 3 − GMFI Tube 1)) ∗ 100. Greater levels of bound VX15/2503 result in a higher GMFI for Tube 2 and higher percent saturation.

Detection of therapeutic antibody in the brain via IHC

For therapeutic antibody detection, 5-μm paraformaldehyde (PFA)-fixed, paraffin-embedded sections were deparaffinized using Xylene baths and rehydrated with graded ethanol baths. Epitope retrieval was carried out by a 20-min boil with Target Retrieval Solution (Dako, Carpinteria, CA) followed by a 30-min cooling period. Slides were washed twice with PBS containing 0.05% Tween-20 (TPBS), then endogenous peroxidases were inactivated with a 10 min block with Dual Enzyme Block (Dako, Carpinteria, CA). Slides were washed with TPBS twice, and nonspecific binding was blocked via a 20-min incubation with 2.5% normal horse serum in TPBS. Following a single TPBS wash, therapeutic antibody (MAb 2B8 or MAb 67-2) was detected with a 60-min incubation with a rat-adsorbed anti-mouse HRP polymer kit (Vector, Burlingame, CA), followed by two TPBS washes and a 5-min DAB+ incubation (Dako, Carpinteria, CA). Sections were then counterstained with Harris hematoxylin, destained, blued with tap water, dehydrated, and non-aqueous mounted with Permount.

Primary rat oligodendrocyte cultures

Oligodendrocyte precursor cells (OPC) were isolated from mixed neuronal cultures obtained from dissociated spinal cord or cortices of P2 rat pups. Briefly, spinal cord or brain cortices were finely chopped and dissociated using a neural tissue dissociation kit (Miltenyi, Cambridge, MA). Dissociated cells were seeded on poly-L-lysine (PLL)-coated T-75 flasks and cultured in DMEM containing 10% FBS/Pen–Strep/gentamicin at 50 mg/ml for 10–14 days. OPC were harvested by shaking the mixed neural culture flasks at 130 rpm overnight at 37 °C. This method routinely yielded 95% pure bipolar A2B5-positive OPC as confirmed by ICC. These OPCs were then cultured for 5–7 days in OPCM (Neurobasal medium (Invitrogen, Grand Island, NY) + B27 serum free supplement (Invitrogen, Grand Island, NY) + 20 ng/ml of human bFGF (Peprotech, Rocky Hill, NJ) + human PDGF (Peprotech, Rocky Hill, NJ) in PLL-coated T-25 dishes.

OPC collapse assay

OPC grown in OPCM were harvested by trypsinization and seeded for a collapse assay on PLL-coated 48-well plates at 1.2×10^4 cells per well. They were cultured in OPCDM (Neurobasal medium + B27 + CTNF (ciliary neurotrophic factor from rat (Sigma, St Loius, MO) (10 ng/ml) + 15 nM Triiodo-L-thyronine (Sigma, St Louis, MO) for 4 days and then treated with either control protein or recombinant his-tagged SEMA4D (rSEMA4D-His) at 50 μg/ml +/− anti SEMA4D antibody (VX15/2503) at 500 μg/ml for 30 min. Treatment was terminated by fixing cells in 4% PFA added directly to treatment wells. Cytoskeletal changes were visualized by staining treated cells with Phalloidin-Alexa488 (Invitrogen, Grand Island, NY) at 1:40 for 30 min post-permeabilization with 0.1% Triton X-100. Actin reorganization was imaged at 20× magnification using an Exi Aqua camera coupled to an Olympus Ix50 microscope.

OPC apoptosis and differentiation assay

OPC grown in OPCM were harvested by trypsinization and seeded at 1.5×10^4 cells per well onto 48-well plates coated with PLL (10 μg/ml) + BSA (50 μg/ml), PLL (10 μg/ml) + SEMA4D (50 μg/ml) or PLL (10 μg/ml) + SEMA4D (50 mg/ml) + anti-SEMA4D (VX15/2503; 250 μg/ml) for 2 h at 22 °C. Cells were cultured in the presence of OPCDM for 4 days for the apoptosis assay or 8 days for the differentiation assay. On day 4 and day 8, cells were fixed with 4% PFA for 20 min and transferred to PBS. The apoptotic cell fraction on day 4 was determined by immunocytochemical staining for activated caspase-3 (Abcam, Cambridge, MA) in the GalCer-positive fraction of plated cells. Differentiation on day 8 was assayed by determining the expression of myelin basic protein (MBP; clone 7D2; Abcam, Cambridge, MA) by immunocytochemistry. Activated caspase 3- and MBP-positive cells were imaged at 20× magnification using an EXi Aqua camera coupled to an Olympus Ix50 microscope. A minimum of 1000 cells/well and 6000 cells/treatment were imaged for each condition and % positive cells quantified using Image-Pro Plus software (MediaCybernetics, Rockville, MD). Data from 6 wells/treatment group were averaged and subjected to statistical analysis (ANOVA) to assess significance.

Lysolecithin lesion model

Focal demyelination in spinal cord was induced by stereotactic infusion of 1% lysophosphatidylcholine (LPC) into a defined level of the rat spinal cord. Briefly, rats were anesthetized with isoflurane and a laminectomy was performed at T9–T10 level. A volume of 2 μl of 1% LPC (Sigma-Aldrich, St. Louis, MO) was injected into the cord at 1 μl/min. Following wound closure, the rats recovered in homeothermic cages before being returned to home cage. At 2 days post-injury, intrathecal cannulation was performed. An incision of the ligamentum flavum between T7 and T8 was made followed by a partial T8 laminectomy. A rat intrathecal catheter (Alzet) filled with either MAb 67-2 or MAb 2B8 solution (7.5 μg/μl) and attached to Alzet minipump (Model #2002 with flow rate of 0.5 μl/h) containing the corresponding dosing solution was then inserted into the subarachnoid space, and the tip of the catheter was advanced caudally to within 1 mm of the injury epicenter. Following implantation and wound closure, rats recovered in homeothermic cages before being returned to home cages. A monoclonal antibody dose of 90 μg/day was infused into the intrathecal space via the Alzet pump at the rate of 0.5 μl/h until end-point day 14 post-LPC infusion. Three rats from LPC-lesioned groups and 3 rats from the sham group were perfused with 4% paraformaldehyde for ex vivo MRI and immunohistochemical analyses. The remaining 9 rats from LPC-lesioned groups and 3 rats from the sham group were perfused with 4% glutaraldehyde for ex vivo MRI and toluidine blue histochemistry

Ex vivo MRI analyses of LPC-lesioned spinal cords

MRI was performed on fixed and dissected spinal columns in a horizontal 7 T magnet with bore size 160 mm equipped with a gradient set capable of maximum gradient strength 750 mT/m and interfaced to a Bruker AVANCE III console (Bruker BioSpin GmbH, Ettlingen, Germany). A volume coil (Bruker Biospin GmbH, Ettlingen, Germany) was used for transmission and surface phased array coil for receiving (Rapid Biomedical GmbH, Rimpar, Germany). Prior to imaging, samples were placed in a tube filled with perfluoro polyether to prevent signal from the solution and fixed to a holder in a standard orientation relative to the magnet bore. For determining the lesion volumes, samples were scanned using a FLASH sequence with the following parameters: Echo Time/Repetition Time (TR/TE) = 1300/3.5 ms, flip angle = 90°, image matrix size = 160 × 160, slice thickness = 0.5 mm, number of slices = 40, field of view (FOV) = 9.6 × 9.6 mm^2 and 24 signal averages per k-space line. Imaging resolution was 60 × 60 × 500 μm^3 and imaging time was for

approximately 1 h. Data were analyzed using in-house written MATLAB software.

Toluidine blue staining and TEM analysis

Naïve rats, LPC-lesioned rats, and rats with EAE and treated with control IgG or anti-SEMA4D were perfused transcardially with heparinized (2.5 IU/ml) phosphate buffer (PB) (0.1 M sodium phosphate buffer, pH 7.2) followed by perfusion with 4% glutaraldehyde diluted in PB. Following perfusion the top of the skull was removed to allow for adequate fixation of the brain. Both the head and spinal column were placed in 4% glutaraldehyde in PB. Five cross sections were cut from each cord, starting at L1 and cutting every 2 mm in a distal direction. Each cross section was post-fixed in osmium tetroxide, processed through a graded series of alcohols, infiltrated into liquid epoxy resin (Epon/Araldite), embedded into molds, and polymerized at 70 °C. Five 1-μm sections were cut from each cross section using an ultramicrotome with a glass knife, which were then stained with Toluidine Blue. Sections were scanned with an Objective Imaging Turboscan system on an Olympus IX50 with a 1.35NA 60× oil objective. To perform a uniform quantitation of all samples, the dorsal column was selected as the area for quantitation in each section. This region has well-defined borders and is enriched for myelinated axons, making it a frequent site of demyelinating events. Additionally, the lumbar region (L1 specifically) was selected based on previous observations that this area of the cord routinely contains lesion loads that correlate with disease severity. For quantitation, the blue channel was extracted from each image, and its histogram equalized using Adobe Photoshop. ImagePro Plus was then used to apply a HiGauss filter to accentuate myelin edges, and the area occupied by myelin stain was then calculated as a percentage for the region of interest (dorsal column). For TEM, the optic nerve and the dorsal column of the spinal cord were selected for further analysis. Thin sections were cut and placed onto grids. Images were captured using a Hitachi 7650 Analytical TEM with an Erlangshen 11-megapixel digital camera and Gatan software.

Statistical analyses

Statistical analysis was performed by means of Student's *t*-test or 2-way analysis of variance (ANOVA) followed by the Bonferroni post-test, when applicable, using GraphPad Prism (GraphPad Software, San Diego, CA).

Results

Antibody to SEMA4D improves clinical scores in multiple EAE models

Because of the potential role(s) of SEMA4D in cellular processes that contribute to pathogenesis in neuroinflammatory and neurodegenerative diseases and because sera from individuals with MS contain on average 2.6 times higher soluble SEMA4D than sera from unaffected individuals (Supplementary Fig. S1), we generated a high affinity antibody to efficiently block the activity of this semaphorin family member in vivo. Using SEMA4D knockout mice, standard immunization and hybridoma methods were employed to select a panel of murine anti-human SEMA4D-specific antibodies. Many of these antibodies were found to cross-react with human, primate, rat and mouse SEMA4D. Antibody produced by hybridoma clone 67-2 (MAb 67-2) exhibited high affinity by surface plasmon resonance (SPR) for both murine ($K_D = 1$ nM) and human recombinant SEMA4D ($K_D = 5.7$ nM). Flow cytometry-based functional studies demonstrated that MAb 67-2 (IgG1) blocked the binding of SEMA4D to PLXNB1, PLXNB2, and CD72 expressed on the surface of transfected cells (data not shown). MAb 67-2 served as the progenitor antibody for the generation of a humanized anti-SEMA4D IgG4 antibody (VX15/2503). Neither MAb 67-2 nor VX15/2503 are cytotoxic in vitro or deplete SEMA4D-positive lymphocytes in vivo (data not shown).

To examine the contribution of SEMA4D to mechanisms underlying neuroinflammatory disease, MAb 67-2 was tested in 4 rodent models of experimental autoimmune encephalomyelitis (EAE): 1) SJL mice immunized with PLP peptide 139-151, 2) adoptive transfer into SJL mice of PLP-peptide primed T cells enriched for Th1 in vitro, 3) C57BL/6 mice immunized with myelin oligodendrocyte glycoprotein (MOG)-peptide 35-55, and 4) Dark Agouti (DA) rat immunized with MOG_{1-125}.

SJL mice develop a relapsing–remitting experimental autoimmune encephalomyelitis (RR-EAE) in response to immunization with a peptide epitope of proteolipid protein ($PLP_{139-151}$) in Complete Freund's Adjuvant (CFA). This model is characterized by a moderate to severe acute paralytic phase followed by remission and subsequent relapses. Treatment of SJL mice with anti-SEMA4D antibody (MAb 67-2) starting 7 to 10 days after $PLP_{139-151}$ immunization reduced the severity of disease by approximately 50% as compared to mice receiving isotype control antibody (MAb 2B8) (Fig. 1A). These results confirm data previously reported by Kumanogoh and colleagues, who described SEMA4D-null mice as exhibiting less severe clinical signs of EAE than their wild-type counterparts (Kumanogoh et al., 2002) and subsequently demonstrated amelioration of EAE in SJL mice by systemic treatment with an independent anti-SEMA4D antibody (Okuno et al., 2010).

In addition to active immunization with myelin peptides, EAE can be induced in SJL mice by adoptive transfer of pre-activated PLP peptide-specific, Th1-polarized T cells (Ishida et al., 2003). In these experiments, splenic $CD4^+$ T cells of SJL donor mice immunized with $PLP_{139-151}$/CFA emulsion were isolated and re-stimulated in vitro with $PLP_{139-151}$ peptide and IL-12 in the presence of anti-IL-4 antibody to enrich for Th1 cells prior to transfer into recipient SJL mice. Administration of anti-SEMA4D antibody starting on day 10 post-adoptive transfer reduced the severity of Th1 cell-mediated EAE relative to mice treated with control IgG. Disease amelioration was comparable to that achieved by treatment with recombinant murine interferon-β (IFN-β; Fig. 1B). Results in this model demonstrate that interference with EAE progression is not simply due to blocking T cell activation.

In contrast to the relapsing–remitting disease induced in SJL mice, EAE induced in C57BL/6 mice by subcutaneous injections of MOG_{35-55} peptide emulsified in CFA induces a chronic course of disease. Treatment with anti-SEMA4D dramatically reduced the group mean score (GMS) of clinical signs of EAE (Fig. 1C). Notably, these experiments were performed in the absence of pertussis toxin which is often employed to potentiate disease in this murine strain. Among other possible pathogenic effects, pertussis toxin compromises the blood–brain barrier (Bruckener et al., 2003) by mechanisms which are distinct from those mediated by inflammatory cells and which appear not to be readily reversed by anti-SEMA4D antibody. As shown in Fig. 1C, even in the absence of pertussis toxin, relatively high clinical scores were induced in control mice.

Immunization of DA rats with whole MOG protein in CFA induces EAE with an acute phase of disease followed by an extended period of chronic neurological deficit and pathology (Mi et al., 2007). Unlike other peptide-based EAE models, anti-MOG antibodies, as well as T cells, are believed to play a key role in the disease that develops in this rat model. Treatment of these animals with anti-SEMA4D resulted in a 32% attenuation in disease severity (Fig. 1D).

Administration of anti-SEMA4D antibody does not result in immunosuppression

Within the normal CNS, SEMA4D is robustly expressed on Nkx2.2-positive oligodendrocyte precursors, while its major receptors, plexin-B1 and CD72, are expressed on multiple cell types and especially prominent on astrocytes which are intimately associated with neurons and microglia (Supplementary Fig. S2). In the setting of EAE, SEMA4D expression can also be readily detected on infiltrating macrophages and

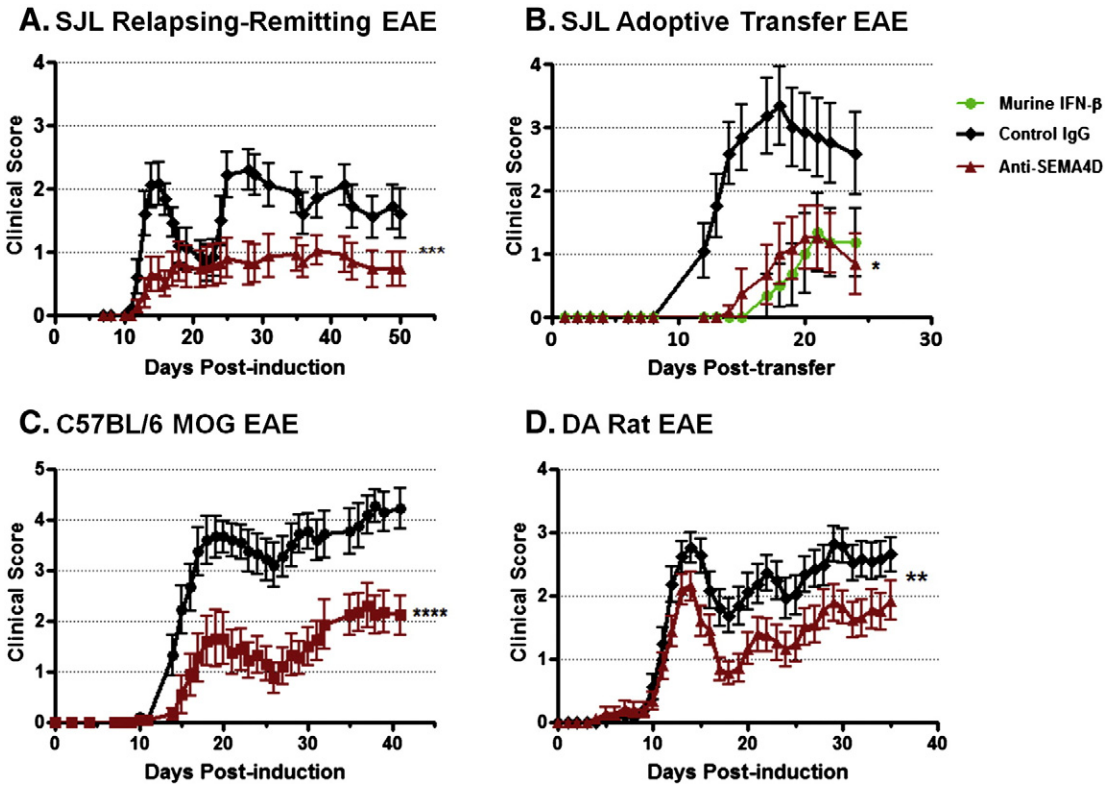

Fig. 1. Anti-SEMA4D antibody treatment significantly improves clinical scores in multiple rodent models of EAE. (A) SJL mice were immunized with myelin proteolipid protein amino acids 139-151 ($PLP_{139-151}$) in Complete Freund's Adjuvant (CFA). Starting on day 7, mice were injected 1× per week with control IgG (MAb 2B8) or anti-SEMA4D (MAb 67-2) antibody (N = 18/group). Standard EAE clinical scoring was performed over a 50-day period. (B) For the Th1 adoptive transfer EAE model, SJL donor mice were immunized with PLP139-151 in CFA. Ten days later CD4 + T cells were isolated from spleens and lymph nodes and were re-stimulated with peptide, IL-12 and anti-IL-4 MAb. After culture and re-stimulation, T cells were transferred into recipient SJL mice. Starting at day 0 post-T cell transfer, mice were injected i.p. weekly with either MAb 2B8 or MAb 67-2, or 3×/week with recombinant murine interferon-beta (IFN-β; N = 12/group), and EAE clinical scores were recorded over a 24-day period. (C) Male C57BL/6 mice were immunized with MOG_{35-55} peptide in CFA (N = 8–9/group). Mice received MAb 2B8 or MAb 67-2 2X/week beginning on day 4 post-MOG immunization, and EAE clinical scores were recorded over a 41-day period. (D) Dark Agouti (DA) rats (N = 30/group) were immunized with MOG_{1-125} in Incomplete Freund's Adjuvant (IFA) containing 200 μg of heat-inactivated *Mycobacterium tuberculosis* (strain H 37 RA). Starting on day 3 post-MOG immunization, rats received MAb 2B8 or MAb 67-2 2×/week up to peak disease (approximately day 14), then 1×/week thereafter. EAE clinical scores were recorded over a 35-day period. Error bars indicate standard error of the mean (SEM). Statistical significance was determined by 2-way ANOVA where "*" = $p < 0.05$, "**" = $p < 0.01$, "****" = $p < 0.005$, and "*****" = $p < 0.0001$.

T cells. In the periphery, SEMA4D is highly expressed on T lymphocytes and to a lesser extent on other immune cells, including B cells, NK cells, and APC and has been shown to play a role in the control of immune cell activation and migration (Delaire et al., 2001; Ishida et al., 2003).

Given the purported role of SEMA4D in immune responses, we investigated whether antibody-mediated neutralization of this semaphorin is immunosuppressive. The immune response profiles engendered against an EAE-inducing peptide were assessed in the presence and absence of anti-SEMA4D antibody treatment in vivo. EAE was actively induced in SJL mice by $PLP_{139-151}$/CFA immunization, and on days 6 and 10 post-immunization mice received control IgG or anti-SEMA4D antibody. At study end, spleens, brains, and spinal cords were processed for ELISPOT, T cell proliferation, and cytokine assays. ELISPOT analysis of $PLP_{139-151}$ re-stimulated mononuclear cells from the spleens of control IgG or anti-SEMA4D treated EAE mice revealed no significant differences in peptide-specific IL-17a or IFNγ release between the groups (Supplementary Fig. S3A). T cell proliferation assays indicated a significant peptide-specific proliferative response was detected with no differences in T cell proliferation between samples obtained from control IgG or anti-SEMA4D treated EAE mice (Supplementary Fig. S3B). Mononuclear cells isolated from spleens and brains/spinal cords of treated and control mice were also analyzed using a cytometric bead array (CBA) kit and flow cytometer. No consistent differences in cytokine levels were seen between treatment and control groups (Supplementary Figs. S3C–D). Peptide-specific responses were most evident when analyzing IFNγ and IL-17 from the mononuclear cells isolated from the brain and spinal cords of both the control and anti-SEMA4D treated groups. Lastly, to determine overall functional immunocompetence, clearance of an infectious microorganism was assessed in the presence of high concentrations of anti-SEMA4D antibody (Gleichmann et al., 1989). Viral clearance was measured in influenza virus-infected rats that had received 5 weekly intravenous injections of varying doses of anti-SEMA4D antibody VX15/2503 prior to virus infection and 3 weekly doses subsequent to infection. VX15/2503, at doses up to 200 mg/kg, did not impair or delay viral clearance in this host resistance model (Supplementary Fig. S4). In aggregate, these data indicate that the improvement in EAE clinical scores observed in anti-SEMA4D treated cohorts is not due to overt suppression of immune responses elicited against EAE-related myelin antigens.

In contrast to the limited effect of anti-SEMA4D antibody on lymphocytes and immune activity, a relatively dramatic inhibition of microglial activation is observed as previously reported by Okuno et al. (27). Spinal cord sections of SJL EAE mice induced by adoptive transfer and treated with either anti-SEMA4D (MAb 67-2) or control IgG (MAb 2B8) were examined for hematoxylin and eosin (H&E) histochemistry and immunohistochemistry for macrophage/microglial markers. H&E staining of representative sections from animals approximating the group mean score in each cohort revealed clearly visible areas of enhanced cellular densities suggestive of immune cell infiltration at sites of EAE lesions (Supplementary Figs. S5A–B). Immunohistochemical analysis of macrophage/microglia using an anti-F4/80 antibody revealed significantly greater staining within the spinal cords of the control IgG cohort as compared to anti-SEMA4D-treated animals (Supplementary Figs. S5C–D). The majority of F4/80-positive cells were CD45 low (data not shown), indicating that these cells were of

microglial and not infiltrating macrophage origin. These results suggest reduced activation and/or migration of microglial cells in animals treated with anti-SEMA4D antibody.

SEMA4D blockade restores blood–brain barrier integrity

It has been previously demonstrated that SEMA4D signaling through the PLXNB1 receptor on endothelial cells induces cytoskeletal rearrangements, cellular activation and migration (Basile et al., 2004; Conrotto et al., 2005). SEMA4D expressed on or released from activated immune cells in neuroinflammatory disease may through these mechanisms compromise the integrity and function of the blood–brain barrier (BBB). The BBB is a highly complex brain endothelial structure of the differentiated neurovascular system comprised of endothelial cells, pericytes and astrocytes. BBB compromise has been implicated in a number of neurodegenerative diseases, including meningitis, brain edema, epilepsy, Alzheimer's disease (AD), Parkinson's disease (PD), stroke, amyotrophic lateral sclerosis (ALS), and MS (reviewed by (Zlokovic, 2011)).

To determine if anti-SEMA4D antibody administration during EAE can protect BBB integrity in vivo, SJL mice were sensitized by immunization with $PLP_{139–151}$/CFA, then treated weekly from day 7 post-induction with either control IgG (MAb 2B8) or anti-SEMA4D (MAb 67-2). On day 13, during the acute phase of the disease, mice were sacrificed and lumbar spinal cord samples were prepared for histopathological analysis of fibrinogen leakage from the microvasculature into CNS interstitial tissue. EAE-related neuropathology was associated with enhanced extravascular leakage of fibrinogen serum protein in lumbar spinal cords (Figs. 2A–C). Anti-SEMA4D antibody-treated EAE mice exhibited greatly diminished fibrinogen leakage within the microvasculature, suggesting that BBB integrity is maintained or restored when SEMA4D is neutralized during the acute phase of disease. Protection of the neurovascular unit and preservation of BBB integrity may contribute to the therapeutic benefit of anti-SEMA4D antibody in neuroinflammatory and neurodegenerative disease.

To further analyze the impact of SEMA4D on BBB, we employed a previously described dynamic in vitro blood–brain barrier (DIV–BBB) model (Cucullo et al., 2011). Briefly, the model consists of hollow polypropylene fibers that contain transcapillary 2 to 4-μm diameter pores. The fibers are connected to a pulsatile pump that facilitates continuous flow of media, cells, and experimental compounds through the fibers. Human brain endothelial cells are inoculated into the luminal compartment and allowed to adhere to and coat the inside walls of the fibers, while human astrocytes are seeded into the abluminal compartment bathing the outside surface of the fibers. The endothelial cells and astrocytes interact across the membrane to induce formation of tight junctions between endothelial cells, the integrity of which can be monitored continuously by measurement of trans-endothelial electrical resistance (TEER). Introduction of increasing concentrations of recombinant SEMA4D (rSEMA4D) into the luminal compartment resulted in decreased TEER values reflecting a breakdown of tight junctions between the cells. Introduction of a control recombinant protein had no impact (data not shown). The breakdown of BBB was reversed within 24 h by the addition of anti-SEMA4D antibody (VX15/2503; Fig. 2D). Introduction of control IgG antibody (MAb 2955) did not affect SEMA4D-induced BBB compromise.

To further investigate the mechanism of SEMA4D induced breakdown of BBB, primary mouse CNS endothelial cultures were established in standard culture plates and were treated with rSEMA4D or with a known BBB disruptor, tumor necrosis factor-alpha (TNFα). Immunocytochemistry was first performed to assess the subcellular localization patterns of the key BBB tight junction protein, Claudin-5 (CLN-5). Untreated cultures exhibited the signature staining pattern for CLN-5 in which the majority of signal was detected on membranes between adjacent endothelial cells (Fig. 2E). Addition of the proinflammatory cytokine TNFα (100 ng/ml for 12 h) resulted in a significant loss of CLN-5, as previously described (Fig. 2F; (Aslam et al., 2012)). Exposure to rSEMA4D (100 ng/ml for 12 h) led to a similar dampening of membrane-associated CLN-5 signal and a partially compensatory enhancement of intracellular compartment staining (Fig. 2G). Homogenates generated from control, TNFα, and rSEMA4D-treated cells after 6 and 12 h of exposure were analyzed by SDS-PAGE and immunoblotting to assess levels of CLN-5. Treatment with either TNFα or rSEMA4D resulted in reduced CLN-5 levels beginning at 6 h and remaining low at 12 h (Figs. 2H and I). These data indicate that SEMA4D promotes breakdown of the BBB via a signaling cascade that involves transient down-regulation of CLN-5 on endothelial cells, and that BBB integrity can be restored by antibody neutralization of SEMA4D.

Anti-SEMA4D penetrates the CNS in the setting of EAE

Since T cells express the highest concentration of membrane SEMA4D, we investigated the level of antibody saturation on T cells within the CNS in EAE-induced SJL mice. T cells were isolated from brains and spinal cords of EAE mice treated with anti-SEMA4D (VX15/2503) or control IgG (MAb 2955). The results show that anti-SEMA4D was bound to recovered T cells at saturation levels up to approximately 90% (Supplementary Figs. S6A–D). However, since T cells circulate and may bind antibody in the periphery, it remained to be determined whether anti-SEMA4D actually penetrates into the CNS in the setting of EAE.

The presence of anti-SEMA4D (MAb 67-2) in cerebellar brain sections from EAE-induced DA rats was immunohistochemically detected using a rat-adsorbed goat anti-mouse antibody (Supplementary Figs. S6E–G). This antibody does not recognize rat IgG, but readily detects the presence of mouse IgG (data not shown). Large areas of antibody penetration into the brain were observed for MAb 67-2 as well as control IgG-treated EAE rats. This staining pattern was not detected in untreated naïve animals. The results demonstrate that antibody can indeed penetrate into brain of EAE rats in antigen-independent fashion.

Effects of SEMA4D on oligodendrocyte precursor cells

Moreau-Fauvarque and colleagues demonstrated SEMA4D expression is up-regulated on oligodendrocytes after spinal cord lesion and that SEMA4D acts as an inhibitor of axonal regeneration (Moreau-Fauvarque et al., 2003). Giraudon et al. have reported that T cell-derived SEMA4D affects immature neural cell survival and blocks process extension (Giraudon et al., 2004). In the setting of stroke, Taniguchi et al. reported that the number of mature oligodendrocytes significantly increases in the brains of both non-ischemic and post-ischemic SEMA4D-deficient mice as compared to wild-type mice (Taniguchi et al., 2009). These reports indicate that SEMA4D signaling is involved in oligodendrocyte development and can play an important role in recovery from CNS injury.

To assess the effects of SEMA4D on the oligodendrocyte lineage and the ability of anti-SEMA4D antibody to promote survival and differentiation of oligodendrocyte precursor cells (OPC), we established OPC cultures and analyzed three physiologic processes central to oligodendrocyte function and viability: actin filament structure, apoptosis, and differentiation. Exposure of OPC cultures to recombinant SEMA4D led to a marked rearrangement in actin filament organization indicative of cytoskeletal collapse, while addition of anti-SEMA4D prevented this cytoskeletal effect (Figs. 3A–D). In companion cultures, recombinant SEMA4D exposure resulted in higher percentages of caspase-3 positive apoptotic cells after 4 days (Fig. 3E) and fewer OPC differentiating into mature MBP-expressing oligodendrocytes after 8 days (Fig. 3F). In each assay, anti-SEMA4D antibody, but not control IgG, reversed these effects to levels similar to BSA-treated negative controls. These in vitro results support previous reports describing a role for SEMA4D signaling in multiple mechanisms central to oligodendrocyte function and viability.

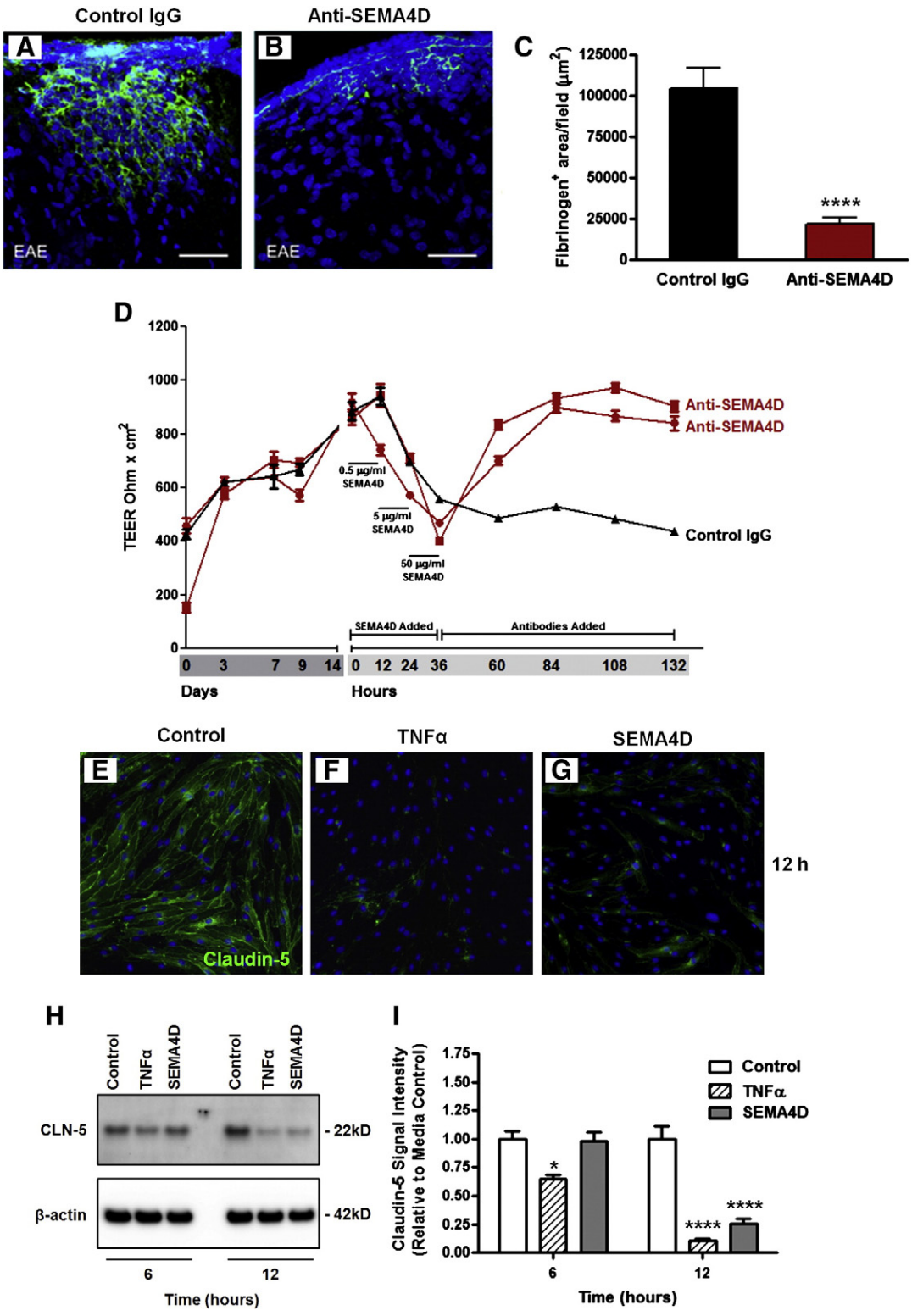

Fig. 2. SEMA4D inhibition preserves integrity of blood–brain barrier. Mice (12 week-old SJL/J; N = 10/group) were sensitized with $PLP_{139–151}$/CFA, then treated once per week from day 7 post-induction with 30 mg/kg control IgG (MAb 2B8; A) or anti-SEMA4D (MAb 67-2; B). On day 13, during the acute phase of the disease, 4 representative mice per group were sacrificed and lumbar spinal cord were analyzed by immunohistochemical staining of fibrinogen, a serum marker of extravascular leakage (A–C). Clinical disease in mice in the control IgG-treated cohort reached a mean disease score of 2.25, while in the anti-SEMA4D-treated group the mean score was 0.75. Scale bars depicted in A and B indicate 50 μm. Statistical significance was determined by Student's *t*-test where "**" = $p < 0.01$ and "***" = $p < 0.001$. The effect of SEMA4D on BBB integrity was subsequently examined in a previously described dynamic in vitro blood–brain barrier (DIV–BBB) model (17). The integrity of the barrier was monitored continuously over the course of the experiment by measurement of transendothelial electrical resistance (TEER; D). At peak TEER (approximately 14 days in vitro), 0.5, 5, and 50 μg/ml recombinant SEMA4D was added successively at 12-h intervals. At 36 h after initial SEMA4D exposure, control IgG (MAb 2955; 1 DIV–BBB unit) or anti-SEMA4D (VX15/2503; 2 DIV–BBB units) was added and TEER measured for another 132 h. Error bars represent standard deviation. The data shown are representative of 3 independent experiments. To assess effects of SEMA4D on tight junction protein Claudin-5 (CLN-5), primary mouse CNS endothelial cultures were left untreated (E) or incubated with 100 ng/ml TNFα as a positive control (F) or recombinant SEMA4D (G) for 12 h, then processed for fluorescence immunocytochemistry (E-G), or treated for 6 or 12 h and subjected to SDS-PAGE and immunoblotting for 22-kDa Claudin-5 and 42-kDa β-actin loading control (H). Gel images were scanned and subjected to densitometry using ImageJ software (I). Error bars indicate standard error. These data are representative of 3 independent experiments.

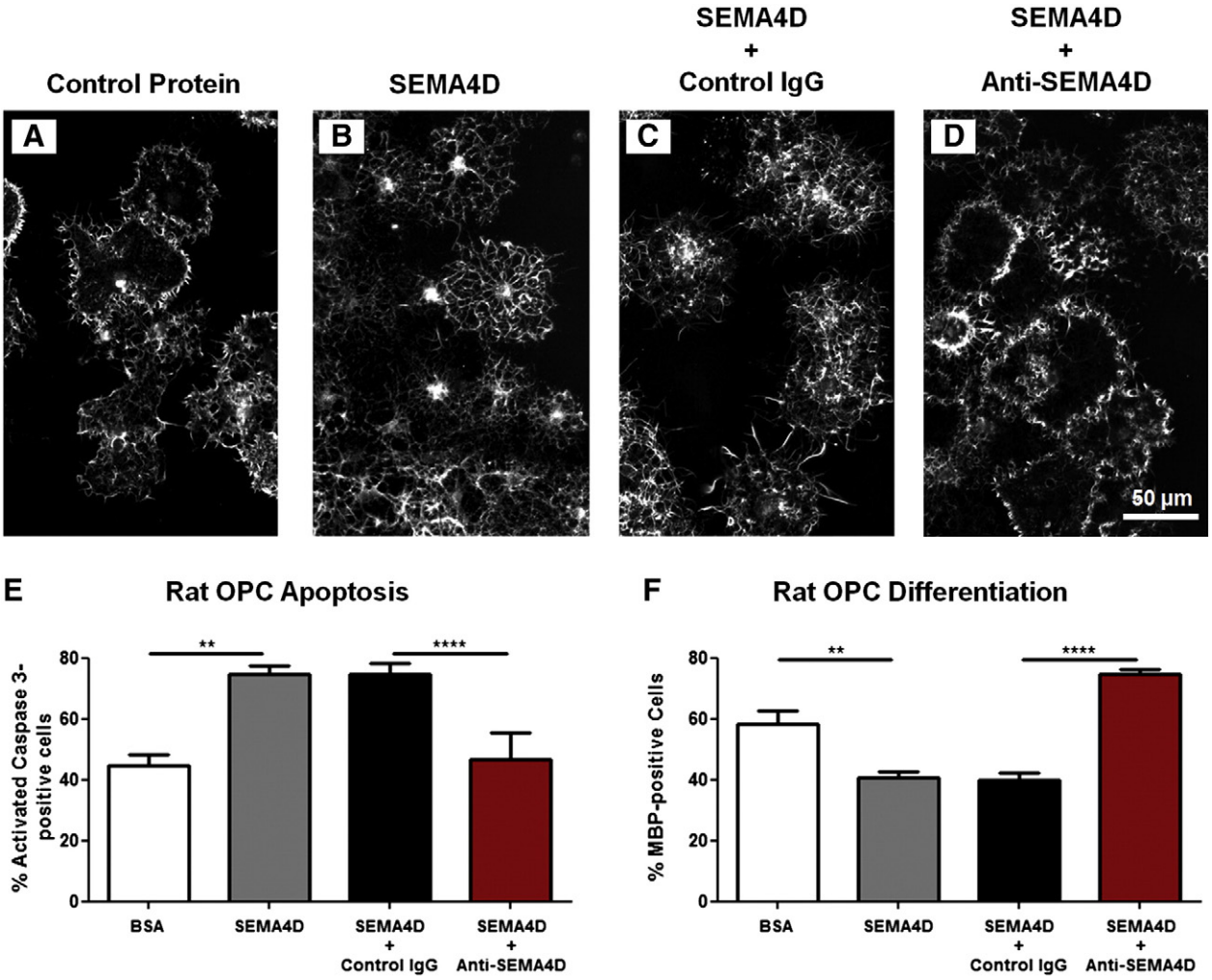

Fig. 3. Anti-SEMA4D rescues oligodendrocyte precursor cells (OPC) from SEMA4D-induced cytoskeletal collapse, apoptosis and inhibition of differentiation. Oligodendrocyte precursor cells (OPCs) were established from dissociated spinal cord or cortices of P2 rat pups. OPCs were seeded for a collapse assay and subsequently treated with control protein (C35 (Evans et al., 2006); A), 50 μg/ml recombinant SEMA4D alone (B), 50 μg/ml SEMA4D + 500 μg/ml control IgG (MAb 2955; C), or 50 μg/ml SEMA4D + 500 μg/ml anti-SEMA4D antibody (VX15/2503; D). Cells were fixed with 4% PFA and cytoskeletal changes were visualized by Phalloidin-A488 staining. Scale bar in D represents 50 μm. For the differentiation assay, OPCs were plated onto wells coated with poly-L-lysine (PLL; 10 μg/ml) + BSA (50 μg/ml), PLL (10 μg/ml) + SEMA4D (50 μg/ml), PLL (10 μg/ml) + SEMA4D (50 μg/ml) + control IgG (MAb 2955; 250 μg/ml), or PLL (10 μg/ml) + SEMA4D (50 mg/ml) + anti-SEMA4D (VX15/2503; 250 μg/ml). (E) Cells were cultured for 4 days and then fixed with 4% PFA and processed for immunohistochemistry to assess extent of apoptosis via enumeration of activated caspase 3-positive cells. (F) Companion cultures were established under an identical set of treatment conditions for 8 days, at which time cells were fixed with 4% PFA and processed for immunohistochemistry to assess number of cells expressing the mature oligodendrocyte marker, myelin basic protein (MBP). Error bars represent standard deviation. Statistical significance was determined by ANOVA with Bonferroni's Multiple Comparison Test where "**" = $p < 0.05$ and "****" = $p < 0.001$.

Anti-SEMA4D treatment improves myelination status in EAE

To examine the impact of anti-SEMA4D in vivo on myelin in antibody-treated EAE animals, we assessed spinal cord myelination status by toluidine blue histochemistry and myelin structural integrity by transmission electron microscopy (TEM). Naïve rats or rats induced to develop EAE and treated with control IgG or anti-SEMA4D were sacrificed and processed for toluidine blue staining or TEM during the chronic phase of disease at day 35 post-recombinant MOG_{1-125}/CFA immunization. A series of toluidine blue-stained spinal cord cross-sections at the level of L1 of the dorsal column substructure were assessed for total myelin content by quantitative image analysis. EAE rats that received anti-SEMA4D (MAb 67-2) harbored significantly more myelinated axons in the dorsal funicular space than those administered control IgG (MAb 2B8; Figs. 4A–E). Areas of EAE-induced demyelination and significant immune cell infiltration were readily apparent in the control IgG-treated EAE cohort (Fig. 4C) and occurred at a higher frequency than in anti-SEMA4D treated EAE rats (Fig. 4D). As shown in Fig. 4E, there is a highly significant difference in percentage of myelin loss in control IgG-treated EAE rats as compared to naïve control animals. Myelination values observed for anti-SEMA4D-treated EAE rats were, in contrast, statistically indistinguishable from those of naïve rats. Examination of dorsal column axons and optic nerve by TEM confirmed the toluidine blue observations and revealed significant differences in myelinated axon ultra-structure between control IgG- (Figs. 4F and I) and anti-SEMA4D-treated EAE animals (Figs. 4G and J), with the latter showing greatly enhanced myelin integrity similar to that observed in naïve control animals (Figs. 4H and K). These results suggest that, in addition to maintaining the integrity of the BBB, anti-SEMA4D antibody directly protects myelin in a neuroinflammatory/neurodegenerative disease.

Anti-SEMA4D treatment enhances myelin repair in lysolecithin-lesioned rats

Lysophosphatidylcholine (LPC; lysolecithin), when stereotactically injected into rat spinal cord, induces demyelinated lesions that undergo a well-characterized process of endogenous remyelination (Pavelko

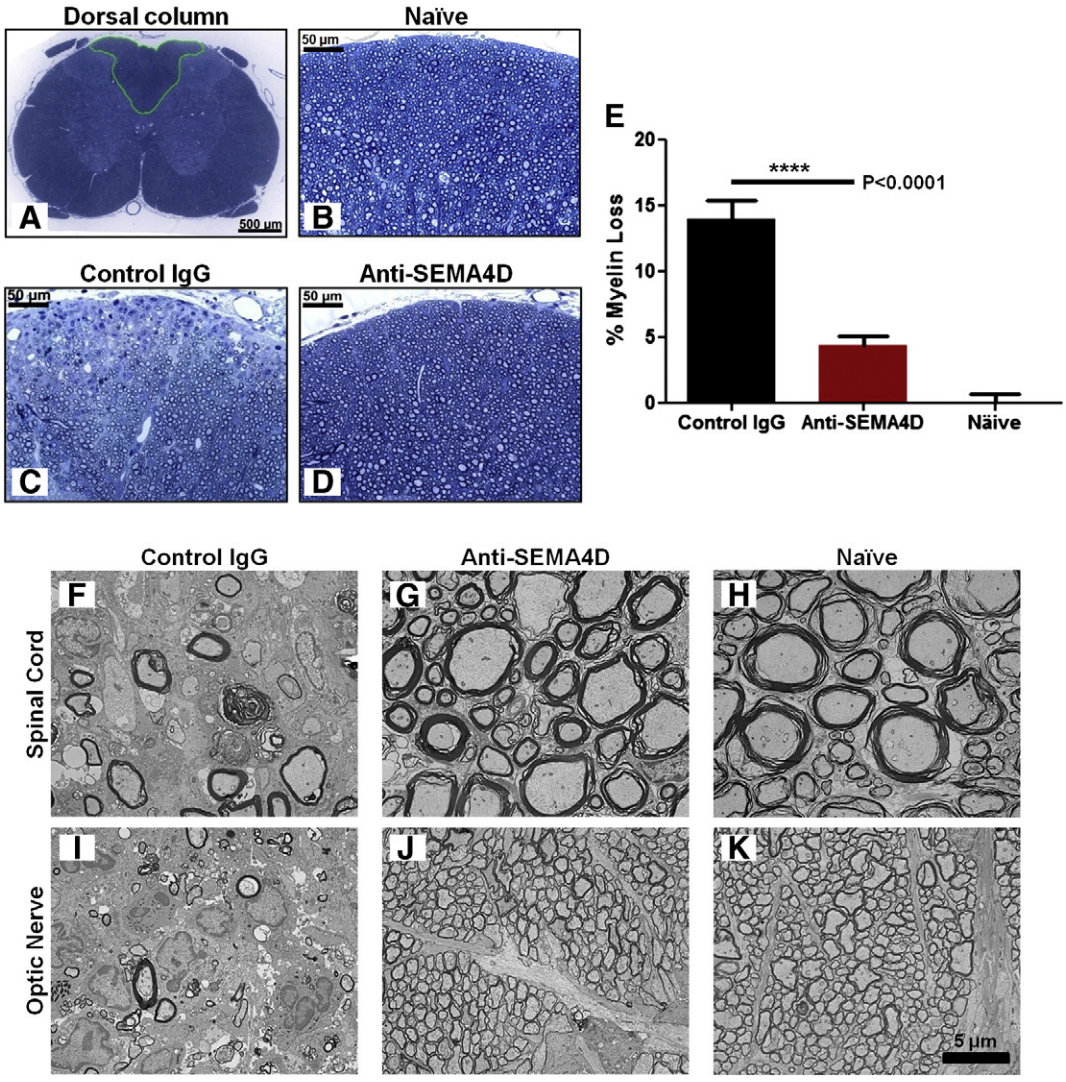

Fig. 4. Protection from EAE-associated demyelination in vivo. To determine the effects of anti-SEMA4D antibody treatment on myelination status, toluidine blue staining was performed on coronal spinal cord sections from naïve rats and antibody-treated, EAE-induced DA rats. Animals received control IgG (MAb 2B8) or anti-SEMA4D (MAb 67-2) 2×/week up to peak disease starting on day 3 post-MOG immunization, then received antibodies 1×/week thereafter. On day 35, mice were sacrificed and processed for toluidine blue histochemistry. Area of myelination (N = 4/group, representative of group mean score) was quantified within the dorsal funiculus (outlined in green; A) for naïve (B), control IgG (C) and anti-SEMA4D-treated rats (D), and represented as % myelin loss (E). Error bars represent standard deviation and "****" indicates $p < 0.0001$ as determined by ANOVA. Scale bar in A equals 500 μm, while those in B–D equal 50 μm. Coronal spinal cord (F–H) and optic nerve sections (I–K) from control IgG (F, I) anti-SEMA4D-treated rats (G, J), and naïve rats (H, K) were also processed for transmission electron microscopy. Scale bar in K represents 5 μm.

et al., 1998). Given that anti-SEMA4D antibody modulates oligodendrocyte precursor cell differentiation and viability in the presence of recombinant SEMA4D in vitro and improves myelin profiles in MAb 67-2 treated EAE rats, we assessed the ability of anti-SEMA4D to enhance remyelination in this timed lesion model, which is not dependent upon peripheral activation of the immune system or significant BBB compromise.. LPC was stereotactically infused into the dorsal funiculus of Sprague–Dawley rat spinal cords, followed 2 days later by implantation of Alzet osmotic pumps that delivered either control IgG or anti-SEMA4D starting on day 3 (90 μg/day; Fig. 5A). Sham control rats were injected with saline instead of LPC and underwent implantation with Alzet pumps that infused control IgG. On day 14 after LPC injection, rats were sacrificed. Spinal columns were removed, lesions imaged by ex vivo magnetic resonance imaging (MRI; Figs. 5B and C), and spinal cord tissue analyzed by TEM and immunohistochemistry. Rats treated with anti-SEMA4D harbored lesions that trended smaller in overall volume ($P = 0.08$; Fig. 5D) and whose MRI-based pixel profiles revealed evidence of diminished severity as compared to control IgG-treated animals (Fig. 5E). Analysis of the outer edge of the lysolecithin lesion using TEM revealed that within the margin of the lesion the anti-SEMA4D treated group harbored more axons with thin myelin in proportion to their axon diameter than rats receiving control IgG infusion (Figs. 5F–H). The G-ratio is the numerical ratio between the diameter of the axon proper and the outer diameter of the myelinated fiber. An increased G-ratio is a distinguishing characteristic of remyelinated axons. Anti-SEMA4D treatment had a dramatic effect on microglial activation and migration of oligodendrocyte precursor cells at the site of lesions as determined by co-immunohistochemistry for Iba1 (for activated microglia; Figs. 6A–C) and Nkx2.2 (for pre-myelinating oligodendrocytes; Figs. 6D–F). Sharply reduced staining for Iba1 indicates reduced activation of inflammatory microglia at the site of lesions as also seen in anti-SEMA4D treated EAE mice (Supplementary Fig. S5) and as previously reported by Okuno et al. (27). Importantly, anti-SEMA4D treatment led to significantly increased numbers of Nkx2.2-positive cells within the lesioned dorsal funiculus (Fig. 6G). Strikingly, there appears to be a redistribution and a concentration of Nkx2.2 positive cells centered in the region of the lesion in sections from anti-SEMA4D treated animals (compare distribution of Nkx2.2 positive

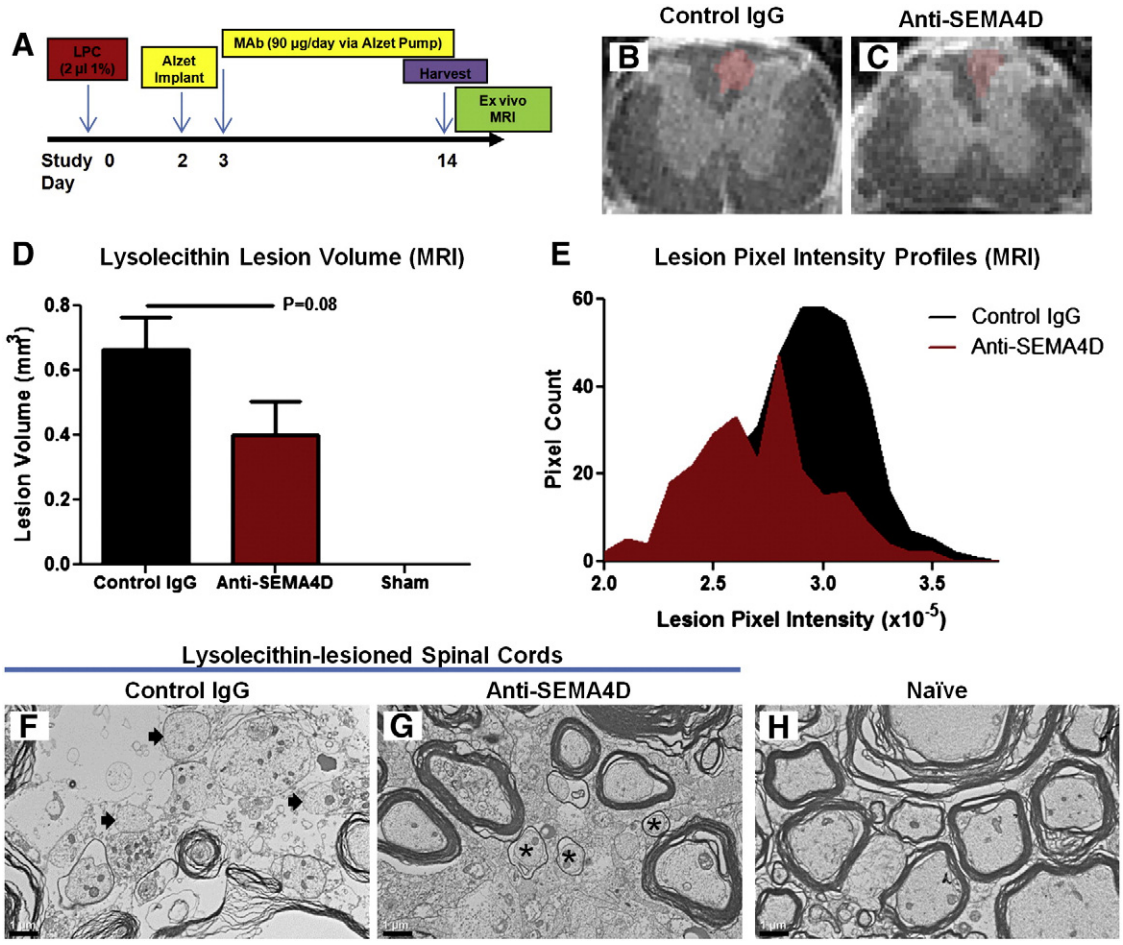

Fig. 5. Anti-SEMA4D delivery improves endogenous remyelination in a lysolecithin-lesioned rat spinal cord. Lysophosphatidylcholine (LPC; lysolecithin) was stereotactically infused into the dorsal funiculus of Sprague–Dawley rat spinal cords (N = 12/group), followed 2 days later by implantation of Alzet osmotic pumps that delivered either control IgG or anti-SEMA4D (90 µg/day; study design schematic shown in A). Sham control rats were injected with saline and underwent implantation with Alzet pumps that infused control IgG (N = 6/group). On day 14 after LPC injection, rats were sacrificed and perfused with 4% glutaraldehyde or 4% paraformaldehyde in saline. Spinal columns were removed, and lesions imaged via ex vivo magnetic resonance imaging (MRI; B and C), and spinal cord tissue analyzed by electron microscopy and immunohistochemistry. Using the MRI imaging data, lesion volumes (D) and pixel intensity profiles (E) were calculated for each rat. Transmission electron microscopy was performed on spinal cord tissue from control IgG (F), anti-SEMA4D (G), and sham operated (H) rats. Scale bars in F–H equal 1 µm. Arrows in F depict demyelinated axons, while asterisks in G demarcate remyelinated axons. Error bars represent standard error and statistical significance was determined using ANOVA.

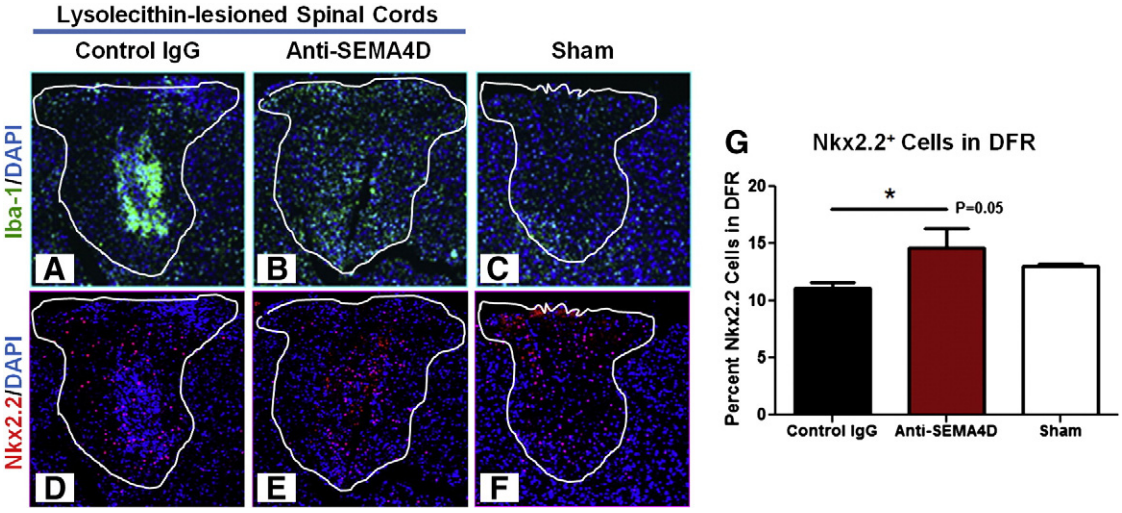

Fig. 6. SEMA4D blockade prevents microglial activation and leads to concentration of Nkx2.2 + oligodendrocytes in region of LPC-induced lesion. To determine if anti-SEMA4D treatment affected the oligodendrocyte lineage in vivo, co-immunohistochemistry for Iba1 (for activated microglia; A–C) and Nkx2.2 (for pre-myelinating oligodendrocytes; D–F) was performed on spinal cord tissue from control IgG (A, D), anti-SEMA4D (B, E), and sham operated (C, F) rats. Numbers of Nkx2.2-positive cells within the dorsal funiculus were calculated (G). Error bars represent standard error and statistical significance was determined using ANOVA, where "*" indicates p = 0.05.

cells in Figs. 6D and E). These data indicate that anti-SEMA4D MAb promotes myelin repair in a model of chemically induced demyelination by mechanisms that result in inducing migration of OPC to the area of lesion or altering the balance of proliferation and apoptosis of Nkx2.2 positive pre-myelinating oligodendrocytes in the region of the lesion. Further investigation will be required to determine whether interactions between activated microglia and OPC play a role in such redistribution.

Discussion

SEMA4D plays a role in multiple cellular processes that contribute to pathophysiology of neuroinflammatory/neurodegenerative diseases and is, therefore, a unique target for therapeutic development. Our findings reported here indicate that anti-SEMA4D antibody may provide therapeutic benefit in the setting of a neuroinflammatory and neurodegenerative disease such as MS via at least two non-mutually exclusive mechanisms: First, anti-SEMA4D prevents SEMA4D-mediated BBB disruption at the level of the microvasculature to impede peripheral cell infiltration and otherwise prevent compromise to the neurovascular unit. Second, anti-SEMA4D prevents the inhibition of migration, survival and differentiation of oligodendrocyte precursor cells and their myelinating function by SEMA4D.

Dysregulated migration of lymphocytes and transendothelial movement of macromolecules across an altered BBB are prominent features of many neuroinflammatory and neurodegenerative disorders, including Alzheimer's disease, Parkinson's disease (PD), stroke, amyotrophic lateral sclerosis (ALS), and MS. The effect of SEMA4D on BBB integrity and the protection afforded by anti-SEMA4D antibody in the setting of EAE are novel findings. SEMA4D signaling through the PLXNB1 receptor has been shown previously to induce cytoskeletal rearrangements and activation and migration of endothelial cells (Basile et al., 2005; Yang et al., 2011). We demonstrated in the DIV–BBB model that SEMA4D can disrupt the integrity of an artificial BBB, and that administration of anti-SEMA4D in either this model or in vivo in EAE can reverse and/or prevent SEMA4D-mediated BBB disruption (Fig. 2). This effect is mediated, at least in part, by preventing SEMA4D-induced changes to the expression or localization of a key tight junction protein, CLN-5. Further experimentation will be needed to finely detail how SEMA4D signaling affects tight junction protein expression and/or subcellular localization in brain microvascular endothelial cells.

Over the course of MS-related disease, there is extensive demyelination that is associated with marked destruction and loss of cells comprising the oligodendrocyte lineage (Ozawa et al., 1994). Endogenous remyelination mechanisms fail during the recovery phase in part because of oligodendrocyte death as well as the inability of OPCs to migrate and differentiate into mature myelinating oligodendrocytes (Wolswijk, 2000). Data obtained from other experimentally induced demyelination models indicate that newly maturing OPCs, in contrast to surviving mature oligodendrocytes, are required for remyelination during the recovery phase (Levine and Reynolds, 1999). Our results confirm those reported by others (Giraudon et al., 2004) of the deleterious effects of SEMA4D signaling on the viability and differentiation capability of OPCs (Fig. 3). After a demyelinating insult, homeodomain transcription factor Nkx2.2 expression has been shown by Watanabe et al. to initially appear in NG2-expressing OPCs surrounding a lesion in vivo and subsequently in both precursors and oligodendrocytes within the lesion prior to the onset of remyelination (Watanabe et al., 2004). Interestingly, intrathecal anti-SEMA4D administration in the timed lysolecithin model led to increased numbers of Nkx2.2-positive cells proximal to the spinal cord lesion (Fig. 6), suggesting that this enhanced migration and concentration of precursors may underlie the improved remyelination observed in this study. It is, however, not clear whether this SEMA4D-mediated activity is a direct effect of SEMA4D expressed on Nkx2.2-positive OPC (Supplementary Fig. S2) or an indirect result of SEMA4D signaling through Plexin-B1 receptor positive CNS-resident glial cells.

Many of the currently available MS therapies are based upon targeted immunosuppression as a means to prevent autoreactive T cells from entering the CNS and further damaging axon-enveloping myelin sheaths. SEMA4D is highly expressed on cells of the immune system and it was possible that antibody-based inhibition of SEMA4D would lead to measurable immune suppression. Indeed, experiments in SEMA4D-deficient (SEMA4D knockout) mice demonstrated reduced antibody responses to T cell-dependent antigens and impaired T cell priming. Both of these functions were restored by administration of exogenous SEMA4D (Shi et al., 2000). Moreover, SEMA4D knockout mice were resistant to the development of EAE due at least in part to a reduced immune response to the EAE-inducing antigen (Kumanogoh et al., 2002). There are, of course, important differences between genetic ablation in a SEMA4D knock-out mouse and anti-SEMA4D treatment in an adult animal with a mature and normal immune system. While we have detected limited effects of anti-SEMA4D antibody on germinal center morphology in repeat dosing studies (data not shown), administration of anti-SEMA4D antibody did not lead to suppression of T cell and cytokine responses to the EAE-inducing peptide (Supplementary Fig. S3) or impede immune clearance of influenza virus infection (Supplementary Fig. S4). Moreover, anti-SEMA4D antibody ameliorates disease in an adoptive transfer model in which myelin-specific T cells are pre-activated in vitro (Fig. 1B) and also improves remyelination status in the lysolecithin model of direct chemically-induced demyelination (Fig. 5). These observations indicate that mechanisms of action other than general immunosuppression are responsible for the clinical benefit observed in anti-SEMA4D antibody-treated EAE animals.

Despite the pleiotropic effects of SEMA4D on BBB integrity, neuronal process extension, and oligodendrocyte differentiation/viability, we did not detect any drug-related side effects/toxicities of anti-SEMA4D antibody in any of our in vivo repeat-dosing studies. Moreover, single and repeat dose toxicity, pharmacokinetic, and pharmacodynamic studies with a humanized anti-SEMA4D (VX15/2503) antibody in cynomolgus monkeys and rats have been completed, with no toxicity observed (manuscript in preparation). Currently, there are 9 FDA-approved, disease-modifying medications for the treatment of MS with purported mechanisms, where defined, mostly related to either impeding T cell traffic to the CNS or inhibiting inflammatory responses. The unique feature of anti-SEMA4D therapy is that it combines independent mechanisms of action that overlap with the anti-inflammatory effects of several of these clinical agents and further extends activity to restoring and protecting the integrity of both BBB and myelinated axons. While approved immunosuppressive and anti-inflammatory drugs have been shown to be effective in transiently suppressing MS-related symptoms and relapse frequency, many have significant side-effects with varying degrees of severity (Weber et al., 2012). In animal studies and ongoing phase 1 clinical trials to date, anti-SEMA4D antibody administration has not been associated with significant overt toxicity.

We have demonstrated that anti-SEMA4D antibody acts through multiple mechanisms to ameliorate a neuroinflammatory/neurodegenerative disease process. Our results show that peripherally administered anti-SEMA4D antibody is active within the CNS in the setting of a severely compromised BBB in EAE. In a separate study to be reported elsewhere (A. Southwell, M. Hayden et al., submitted for publication), we confirm striking protection of both gray and white matter in a transgenic Huntington's disease model, a disease setting with much more limited inflammation or compromise to BBB. This may be relevant to treatment of progressive forms of MS which, although they exhibit endothelial cell abnormalities within CNS vasculature, do not show evidence of BBB compromise that is as severe or extensive as that observed in relapsing forms of the disease (Soon et al., 2007; Leech et al., 2007). In summary, we have developed an antibody-based therapeutic to inhibit SEMA4D signaling as a novel strategy to treat neuroinflammatory/neurodegenerative diseases. The drug target, semaphorin 4D, participates in multiple cellular

processes, including BBB integrity, microglial activation, and oligodendrocyte function, which are known to contribute to the pathophysiology of a number of debilitating neuroinflammatory and neurodegenerative diseases.

Supplementary data to this article can be found online at http://dx.doi.org/10.1016/j.nbd.2014.10.008.

Funding

This work was supported by Vaccinex, Inc.

Author contributions

ESS and MZ conceived the project; all authors contributed to experimental design and the critical discussion of the data; and ESS, WJB and MZ wrote the manuscript.

Competing interests

Vaccinex, Inc., a private Delaware corporation, has patent rights based on inventions described in this publication and is developing a humanized anti-SEMA4D antibody for clinical use. ESS, AJ, CR, JV, TF, MD, EK, CM, CC, JS, HB, ST, RK, AH, EEE, MP, WJB, and MZ are employees of Vaccinex, Inc. Mount Sinai School of Medicine and Cleveland Clinic Lerner College of Medicine received research support from Vaccinex for experimental work related to this project performed in the laboratories of GJ and DJ, respectively. All other authors, NM, ATA, and TP declare no competing interests.

Acknowledgments

The authors would like to thank their colleagues Laurie A. Winter, Tracy Pandina, Christina M. Dewit, Chaitali Ghosh, Loretta L. Mueller, Patrick Kenney, Leslie A. Balch, Maria Scrivens, Gail Seigel, and Susan M. Giralico for stimulating discussion and technical assistance.

References

Adams, C.W., 1977. Pathology of multiple sclerosis: progression of the lesion. Br. Med. Bull. 33, 15–20.
Aslam, M., Ahmad, N., Srivastava, R., Hemmer, B., 2012. TNF-alpha induced NFkappaB signaling and p65 (RelA) overexpression repress Cldn5 promoter in mouse brain endothelial cells. Cytokine 57, 269–275.
Axtell, R.C., deJong, B.A., Boniface, K., van der Voort, L.F., Bhat, R., DeSarno, P., et al., 2010. T helper Type 1 and 17 cells determine efficacy of interferon-B in MS & experimental encephalomyelistis. Nat. Med. 16, 406–412.
Azzarelli, R., Pacary, E., Garg, R., Garcez, P., van den Berg, D., Riou, P., et al., 2014. An antagonistic interaction between PlexinB2 and Rnd3 controls RhoA activity and cortical neuron migration. Nat. Commun. 5, 3405.
Basile, J.R., Barac, A., Zhu, T., Guan, K.L., Gutkind, J.S., 2004. Class IV semaphorins promote angiogenesis by stimulating Rho-initiated pathways through plexin-B. Cancer Res. 64, 5212–5224.
Basile, J.R., Afkhami, T., Gutkind, J.S., 2005. Semaphorin 4D/plexin-B1 induces endothelial cell migration through the activation of PYK2, Src, and the phosphatidylinositol 3-kinase-Akt pathway. Mol. Cell. Biol. 25, 6889–6898.
Basile, J.R., Gavard, J., Gutkind, J.S., 2007. Plexin-B1 utilizes RHOA and ROK to promote the integrin-dependent activation of AKT and ERK, and endothelial cell motility. J. Biol. Chem. 282, 34888–34895.
Berger, J.R., 2010. Progressive multifocal leukoencephalopathy and newer biological agents. Drug Saf. 33, 969–983.
Brinkmann, V., Billich, A., Baumruker, T., Heining, P., Schmouder, R., Francis, G., et al., 2010. Fingolimod (FTY720): discovery and development of an oral drug to treat multiple sclerosis. Nat. Rev. Drug Discov. 9, 883–897.
Bruckener, K.E., el, B.A., Galla, H.J., Schmidt, M.A., 2003. Permeabilization in a cerebral endothelial barrier model by pertussis toxin involves the PKC effector pathway and is abolished by elevated levels of cAMP. J Cell Sci. 116, 1837–1846.
Ch'ng, E.S., Kumanogoh, A., 2010. Roles of Sema4D and Plexin-B1 in tumor progression. Mol. Cancer 9, 251.
Conrotto, P., Valdembri, D., Corso, S., Serini, G., Tamagnone, L., Comoglio, P.M., et al., 2005. Sema4D induces angiogenesis through Met recruitment by Plexin B1. Blood 105, 4321–4329.
Cucullo, L., Marchi, N., Hossain, M., Janigro, D., 2011. A dynamic in vitro BBB model for the study of immune cell trafficking into the central nervous system. J. Cereb. Blood Flow Metab. 31, 767–777.
Delaire, S., Billard, C., Tordjman, R., Chedotal, A., Elhabazi, A., Bensussan, A., et al., 2001. Biological activity of soluble CD100. II. Soluble CD100, similarly to H-SemaIII, inhibits immune cell migration. J. Immunol. 166, 4348–4354.
Errede, M., Girolamo, F., Ferrara, G., Strippoli, M., Morando, S., Boldrin, V., et al., 2012. Blood–brain barrier alterations in the cerebral cortex in experimental autoimmune encephalomyelitis. J. Neuropathol. Exp. Neurol. 71, 840–854.
Evans, E.E., Henn, A.D., Jonason, A., Paris, M.J., Schiffhauer, L.M., Borrello, M.A., et al., 2006. C35 (C17orf37) is a novel tumor biomarker abundantly expressed in breast cancer. Mol. Cancer Ther. 5, 2919–2930.
Giger, R.J., Hollis, E.R., Tuszynski, M.H., 2010. Guidance molecules in axon regeneration. Cold Spring Harb. Perspect. Biol. 2, a001867.
Giordano, S., Corso, S., Conrotto, P., Artigiani, S., Gilestro, G., Barberis, D., et al., 2002. The semaphorin 4D receptor controls invasive growth by coupling with Met. Nat. Cell Biol. 4, 720–724.
Giraudon, P., Vincent, P., Vuaillat, C., Verlaeten, O., Cartier, L., Marie-Cardine, A., et al., 2004. Semaphorin CD100 from activated T lymphocytes induces process extension collapse in oligodendrocytes and death of immature neural cells. J. Immunol. 172, 1246–1255.
Giraudon, P., Vincent, P., Vuaillat, C., 2005. T-cells in neuronal injury and repair: semaphorins and related T-cell signals. Neruomol. Med. 7, 207–216.
Gleichmann, E., Kimber, I., Purchase, I.F., 1989. Immunotoxicology: suppressive and stimulatory effects of drugs and environmental chemicals on the immune system. A discussion. Arch. Toxicol. 63, 257–273.
Hall, K.T., Boumsell, L., Schultze, J.L., Boussiotis, V.A., Dorfman, D.M., Cardoso, A.A., et al., 1996. Human CD100, a novel leukocyte semaphorin that promotes B-cell aggregation and differentiation. Proc. Natl. Acad. Sci. U. S. A. 93, 11780–11785.
Hohlfeld, R., Barkhof, F., Polman, C., 2011. Future clinical challenges in multiple sclerosis: relevance to sphingosine 1-phosphate receptor modulator therapy. Neurology 76, S28–S37.
Ishida, I., Kumanogoh, A., Suzuki, K., Akahani, S., Noda, K., Kikutani, H., 2003. Involvement of CD100, a lymphocyte semaphorin, in the activation of the human immune system via CD72: implications for the regulation of immune and inflammatory responses. Int. Immunol. 15, 1027–1034.
Jager, A., Dardalhon, V., Sobel, R.A., Bettelli, E., Kuchroo, V.K., 2009. Th1, Th17, and Th9 effector cells induce experimental autoimmune encephalomyelitis with different pathological phenotypes. J. Immunol. 183, 7169–7177.
Kappos, L., Radue, E.W., O'Connor, P., Polman, C., Hohlfeld, R., Calabresi, P., et al., 2010. A placebo-controlled trial of oral fingolimod in relapsing multiple sclerosis. N. Engl. J. Med. 362, 387–401.
Kikutani, H., Kumanogoh, A., 2003. Semaphorins in interactions between T cells and antigen-presenting cells. Nat. Rev. Immunol. 3, 159–167.
Kumanogoh, A., Kikutani, H., 2001. The CD100–CD72 interaction: a novel mechanism of immune regulation. Trends Immunol. 22, 670–676.
Kumanogoh, A., Watanabe, C., Lee, I., Wang, X., Shi, W., Araki, H., et al., 2000. Identification of CD72 as a lymphocyte receptor for the class IV semaphorin CD100: a novel mechanism for regulating B cell signaling. Immunity 13, 621–631.
Kumanogoh, A., Suzuki, K., Ch'ng, E., Watanabe, C., Marukawa, S., Takegahara, N., et al., 2002. Requirement for the lymphocyte semaphorin, CD100, in the induction of antigen-specific T cells and the maturation of dendritic cells. J. Immunol. 169, 1175–1181.
Leech, S., Kirk, J., Plumb, J., McQuaid, S., 2007. Persistent endothelial abnormalities and blood–brain barrier leak in primary and secondary progressive multiple sclerosis. Neuropathol. Appl. Neurobiol. 33, 86–98.
Levine, J.M., Reynolds, R., 1999. Activation and proliferation of endogenous oligodendrocyte precursor cells during ethidium bromide-induced demyelination. Exp. Neurol. 160, 333–347.
Liang, X., Draghi, N.A., Resh, M.D., 2004. Signaling from integrins to Fyn to Rho family GTPases regulates morphologic differentiation of oligodendrocytes. J. Neurosci. 24, 7140–7149.
Mi, S., Hu, B., Hahm, K., Luo, Y., Kam Hui, E.S., Yuan, Q., et al., 2007. LINGO-1 antagonist promotes spinal cord remyelination and axonal integrity in MOG-induced experimental autoimmune encephalomyelitis. Nat. Med. 13, 1228–1233.
Miller, D.H., Khan, O.A., Sheremata, W.A., Blumhardt, L.D., Rice, G.P., Libonati, M.A., et al., 2003. A controlled trial of natalizumab for relapsing multiple sclerosis. N. Engl. J. Med. 348, 15–23.
Moreau-Fauvarque, C., Kumanogoh, A., Camand, E., Jaillard, C., Barbin, G., Boquet, I., et al., 2003. The transmembrane semaphorin Sema4D/CD100, an inhibitor of axonal growth, is expressed on oligodendrocytes and upregulated after CNS lesion. J. Neurosci. 23, 9229–9239.
Niederost, B., Oertle, T., Fritsche, J., McKinney, R.A., Bandtlow, C.E., 2002. Nogo-A and myelin-associated glycoprotein mediate neurite growth inhibition by antagonistic regulation of RhoA and Rac1. J. Neurosci. 22, 10368–10376.
Okuno, T., Nakatsuji, Y., Moriya, M., Takamatsu, H., Nojima, S., Takegahara, N., et al., 2010. Roles of Sema4D–Plexin-B1 interactions in the central nervous system for pathogenesis of experimental autoimmune encephalomyelitis. J. Immunol. 184, 1499–1506.
Ozawa, K., Suchanek, G., Breitschopf, H., Bruck, W., Budka, H., Jellinger, K., et al., 1994. Patterns of oligodendroglia pathology in multiple sclerosis. Brain 117, 1311–1322.
Pavelko, K.D., van Engelen, B.G., Rodriguez, M., 1998. Acceleration in the rate of CNS remyelination in lysolecithin-induced demyelination. J. Neurosci. 18, 2498–2505.
Pierson, E., Simmons, S.B., Castelli, L., Goverman, J.M., 2012. Mechanisms regulating regional localization of inflammation during CNS autoimmunity. Immunol. Rev. 248, 205–215.
Prineas, J., 1975. Pathology of the early lesion in multiple sclerosis. Hum. Pathol. 6, 531–554.

Shi, W., Kumanogoh, A., Watanabe, C., Uchida, J., Wang, X., Yasui, T., et al., 2000. The class IV semaphorin CD100 plays nonredundant roles in the immune system: defective B and T cell activation in CD100-deficient mice. Immunity 13, 633–642.

Soon, D., Tozer, D., Altmann, D., Tofts, P., Miller, D., 2007. Quantification of subtle blood–brain barrier disruption in non-enhancing lesions in multiple sclerosis: a study of disease and lesion subtypes. Mult. Scler. 13, 884–894.

Suzuki, K., Kumanogoh, A., Kikutani, H., 2008. Semaphorins and their receptors in immune cell interactions. Nat. Immunol. 9, 17–23.

Tamagnone, L., Artigiani, S., Chen, H., He, Z., Ming, G.I., Song, H., et al., 1999. Plexins are a large family of receptors for transmembrane, secreted, and GPI-anchored semaphorins in vertebrates. Cell 99, 71–80.

Taniguchi, Y., Amazaki, M., Furuyama, T., Yamaguchi, W., Takahara, M., Saino, O., et al., 2009. Sema4D deficiency results in an increase in the number of oligodendrocytes in healthy and injured mouse brains. J. Neurosci. Res. 87, 2833–2841.

Vos, C.M., Geurts, J.J., Montagne, L., van Haastert, E.S., Bo, L., van, d., V, et al., 2005. Blood–brain barrier alterations in both focal and diffuse abnormalities on postmortem MRI in multiple sclerosis. Neurobiol. Dis 20, 953–960.

Watanabe, M., Hadzic, T., Nishiyama, A., 2004. Transient upregulation of Nkx2.2 expression in oligodendrocyte lineage cells during remyelination. Glia 46, 311–322.

Weber, M.S., Menge, T., Lehmann-Horn, K., Kronsbein, H.C., Zettl, U., Sellner, J., et al., 2012. Current treatment strategies for multiple sclerosis — efficacy versus neurological adverse effects. Curr. Pharm. Des. 18, 209–219.

Wolswijk, G., 2000. Oligodendrocyte survival, loss and birth in lesions of chronic-stage multiple sclerosis. Brain 123, 105–115.

Yang, Y.H., Zhou, H., Binmadi, N.O., Proia, P., Basile, J.R., 2011. Plexin-B1 activates NF-kappaB and IL-8 to promote a pro-angiogenic response in endothelial cells. PLoS ONE 6, e25826.

Zhu, L., Bergmeier, W., Wu, J., Jiang, H., Stalker, T.J., Cieslak, M., et al., 2007. Regulated surface expression and shedding support a dual role for semaphorin 4D in platelet responses to vascular injury. Proc. Natl. Acad. Sci. U. S. A. 104, 1621–1626.

Zlokovic, B.V., 2011. Neurovascular pathways to neurodegeneration in Alzheimer's disease and other disorders. Nat. Rev. Neurosci. 12, 723–738.